DOKUZ EYLÜL UNIVERSITY
GRADUATE SCHOOL OF NATURAL AND APPLIED SCIENCES

ENERGY, EXERGY AND TECHNO-ECONOMIC ANALYSES OF SYNTHETIC FUEL PRODUCTION IN A GEOTHERMAL POWER PLANT

by

Doğukan Süleyman MIZRAK

September, 2025

İZMİR

ENERGY, EXERGY AND TECHNO-ECONOMIC ANALYSES OF SYNTHETIC FUEL PRODUCTION IN A GEOTHERMAL POWER PLANT

A Thesis Submitted to the
Graduate School of Natural and Applied Sciences of Dokuz Eylül University
In Partial Fulfillment of the Requirements for Master of Science in
Department of Mechanical Engineering, Thermodynamics Program

by

Doğukan Süleyman MIZRAK

September, 2025

İZMİR

M.Sc THESIS EXAMINATION RESULT FORM

We have read the thesis entitled **"ENERGY, EXERGY AND TECHNO-ECONOMIC ANALYSIS OF SYNTHETIC FUEL PRODUCTION IN A GEOTHERMAL POWER PLANT"** completed by **DOĞUKAN SÜLEYMAN MIZRAK** under supervision of **PROF.DR. CAN ÖZGÜR ÇOLPAN** and **ASST.PROF.DR. YAĞMUR NALBANT ATAK** and we certify that in our opinion it is fully adequate, in scope and in quality, as a thesis for the degree of Master of Science.

Prof.Dr. Can Özgür ÇOLPAN

Supervisor

Prof.Dr. Arif HEPBAŞLI

Jury Member

Prof.Dr. Aytunç EREK

Jury Member

Prof. Dr. Abdullah SEÇGİN

Director

Graduate School of Natural and Applied Sciences

ACKNOWLEDGMENT

The author wishes to express profound gratitude to co-supervisors Prof. Dr. Can Özgür ÇOLPAN and Asst.Prof.Dr. Yağmur Nalbant Atak for their invaluable supervision, advice, encouragement, support, and insight throughout the research process.

The author wishes to express her special thanks to his dear friends, Anıl ERDOĞAN and Alper Can İNCE, for their valuable contributions to this study.

The author also thanks all Mechanical Engineering Department faculty members for their instructions during his graduate studies.

The author also thanks all faculty members of the esteemed jury members for their valuable time.

The author gratefully thanks her parents, Nurgül MIZRAK and Şehmuz MIZRAK, especially his sister Selin MIZRAK and his wife Merve MIZRAK, for their invaluable support throughout her entire life.

Doğukan Süleyman MIZRAK

ENERGY, EXERGY AND TECHNO-ECONOMIC ANALYSES OF SYNTHETIC FUEL PRODUCTION IN A GEOTHERMAL POWER PLANT

ABSTRACT

This study presents the thermodynamic and techno-economic analysis of a geothermal-powered integrated system for synthetic methane production. In this system, the carbon dioxide contained in the non-condensable gas stream, which is the output of the geothermal system, is captured and converted into synthetic methane through the methanation (Sabatier) reaction. In the study, a portion of the captured carbon dioxide is fed to the Sabatier reactor, where it reacts with hydrogen produced by an electrolyser that is also integrated into the geothermal system, resulting in synthetic methane production. The excess carbon dioxide not used for methanation is compressed and reinjected into the reservoir, thus maintaining good integrity and sustainability. The effects of the production well temperature, working fluid type used in the Organic Rankine Cycle and the operating temperature of the Sabatier reactor on the amount of methane produced, the thermal and exergy efficiency of the integrated power-methane production system are analyzed in detail. Additionally, the effect of the electrolyzer's capacity on the net power production and the system's thermal and exergy efficiencies was also investigated. Techno-economic analysis of the PTG system was performed, including the system's Payback Period (SPP) and Levelized Cost of Methane (LCOM) calculations. The mathematical model developed using the Engineering Equation Solver (EES) demonstrates that the R290 refrigerant provided the highest thermal and exergy efficiency. This study indicated that geothermal power plants can be integrated with systems capable of producing synthetic fuels, not limited solely to electricity generation. Moreover, it demonstrated that such multifunctional systems could contribute to carbon reduction and provide a viable solution for sustainable energy production.

Keywords: Geothermal energy, synthetic methane, Sabatier reactor, organic rankine cycle, thermo-economic analysis, electrolyser, carbon dioxide conversion

JEOTERMAL GÜÇ SANTRALİNDE SENTETİK YAKIT ÜRETİMİNİN ENERJİ, EKSERJİ TEKNO-EKONOMIK ANALİZİ

ÖZ

Bu çalışma sentetik metan üretimi yapan ve jeotermal güç santraline entegre edilen bir sistemin termodinamik ve tekno-ekonomik analizini içermektedir. Sentetik metan üretim süreci jeotermal sistemin çıktısı olan ve yoğuşmayan gazlar olarak nitelendirilen gaz akışının içerisinde bulunan karbondioksitin yakalanarak metanasyon reaksiyonu ile sentetik metana dönüştürülesini kapsamaktadır. Çalışmada yakalanan karbondioksitin bir kısmı Sabatier reaktörüne gönderilmekte, yine jeotermal sisteme entegre edilen bir elektrolizörden elde edilen hidrojen ile tepkimesi sonucunda sentetik metan üretimi yapıldığı gösterilmiştir. Sentetik metan üretimi için gereken karbondioksitin fazlası yine basınçlandırma yapılarak tekrardan kuyuya geri gönderilmekte böyleylikle kuyu sağlığı ve devamlılığıda sağlanmaktadır. Rezervuar sıcaklığının, Organik Rankine Çevriminde kullanılan çalışma sıvısı türünün ve Sabatier reaktörünün çalışma sıcaklığının üretilen metan miktarı ve entegre güç-metan üretim sisteminin termal ve ekserji verimliliği üzerindeki etkileri ayrıntılı olarak analiz edilmiştir. Ayrıca, elektrolizörün kapasitesinin net güç üretimi ve sistemin genel termal ve ekserji verimliliği üzerindeki etkisi de araştırılmıştır. PTG sisteminin geri ödeme süresi ve metan maliyetinin seviyelendirilmesi hesaplamaları da dahil olmak üzere, sistemin tekno-ekonomik analizi gerçekleştirilmiştir. EES kullanılarak oluşturulan matematik model ile R290 gazının en yüksek verimliliği sağladığı gösterilmiştir. Bu çalışma, jeotermal enerjinin tesislerinin sadece elektrik üretimiyle sınırlı kalmayıp, sentetik yakıt üretimi yapabilen bir sistemle entegre edilebileceğini göstermekte buna ek olarak çok daha işlevli ve karbon azaltımına yönelikte bir sorun çözücü sistemlere evrilebileceğini ortaya koymaktadır.

Anahtar kelimeler: Jeotermal enerji, sentetik metan, sabatier reaktörü, organik rankine çevrimi, termoekonomik analiz, elektrolizör, karbon dioksit dönüşümü

CONTENTS

Page

M.Sc THESIS EXAMINATION RESULT FORM ii
ACKNOWLEDGMENT iii
ABSTRACT iv
ÖZ v
CONTENTS vi
LIST OF FIGURES ix
LIST OF TABLES x

CHAPTER ONE - INTRODUCTION 1

1.1 Introduction 1
1.2 Motivation 2
1.3 Objective 2
1.4 Thesis Outline 3

CHAPTER TWO - BACKGROUND AND LITERATURE REVIEW 4

2.1 Introduction 4
2.2 Renewable Energy 4
2.2.1 Geothermal Energy 6
2.2.1.1 Exploring Geothermal Energy's Contribution to Sustainable Power Generation 8
2.2.1.2 Working Principle and System Types of Geothermal Systems 11
2.3 Non-Condensable Gases 17
2.4 Sabatier Reaction 19
2.5 Electrolyser 20

CHAPTER THREE - MATHEMATICAL MODELLING OF SYNTHETIC METHANE PRODUCTION SYSTEM 26

3.1 Introduction 26

3.2 System Description 26
3.3 Modelling of the Geothermal Power Plant 27
3.3.1 Selection of the Geothermal Fluid 28
3.3.2 Heat Exchanger 28
3.3.3 Turbine and Generator 31
3.3.4 Air Cooled Condenser and Pump 32
3.4 Modelling of the Proton Exchange Membrane Electrolyser 33
3.5 Modelling of the Carbon Dioxide Capture System 34
3.6 Modelling of the Sabatier Reactor 35
3.7 Calculation of the Thermal Efficiency of the System 37
3.7 Exergy Analysis of the System 38
3.7.1 Physical Exergy 39
3.7.2 Chemical Exergy 39
3.7.3 Exergy Balance 40
3.7.4 Exergetic Performance Assessment 41

CHAPTER FOUR-TECHNO ECONOMIC ANALYSIS OF SYSTEM 43

4.1 Introduction 43
4.3 CAPEX (Capital Expenditure) Costs 45
4.3 OPEX (Operational Expenditure) Costs 48
4.4 Calculation of Levelized Costs 48

CHAPTER FIVE - RESULTS AND DISSCUSSION 50

5.1 Introduction 50
5.2 Effect of the Working Fluid of the ORC 50
5.3 Effect of Reaction Temperature on the Reaction 52
5.4 Effect of Electrolyser Capacity on the System Efficiency 53
5.4 Effect of Production Well Temperature on the System Efficiency 54
5.5 Exergy Destruction Calculation for the Each Component at the System 55
5.6 Techno-Economic Results of the System 57

CHAPTER SIX - CONCLUSIONS 59

REFERENCES 62

LIST OF FIGURES

Page

Figure 2.1 Renewable energy production of the different types of plants 6

Figure 2.2 Geothermal gradient and Earth's interior layers..... 7

Figure 2.3 Dry steam geothermal power plants 15

Figure 2.4 Flash steam geothermal power plants..... 16

Figure 2.5 Binary geothermal power plants..... 17

Figure 2.6 Alkaline electrolysers working scheme 21

Figure 2.7 PEM electrolyser working scheme 22

Figure 2.8 Schematic view of solid oxide water electrolysis working principle 23

Figure 2.9 An NCG system integrated into a flash steam power plant..... 25

Figure 3.1 Schematic view of the power to synthetic methane system..... 27

Figure 3.2 Schematic view of the shell and tube type heat exchanger..... 31

Figure 4.1 Cash flow diagram of the plant during the lifetime..... 47

Figure 5.1 Effect of different ORC working fluids on the energy efficiency and net power output of the integrated system 51

Figure 5.2 Effect of Sabatier reactor temperature on the molar fraction of species .. 53

Figure 5.3 Effect of electrolyser capacity on the system efficiency 54

Figure 5.4 Effect of production well temperature on the net power output, exergy and thermal efficiency……...55

Figure 5.5 Exergy destructions of each component in the integrated system…….56

Figure 5.6 Exergy destruction rates of each component in the integrated system on the Sankey Diagram…….56

LIST OF TABLES

Page

Table 2.1 Evolution of the geothermal power usage ……..…….7

Table 2.2 Evolution of geothermal power worldwide in the last 43 years..... 9

Table 2.3 Changes in geothermal installed capacity and generation in the last 3 years 10

Table 2.4 Classification of the geothermal reservoir 13

Table 2.5 Different ORC working fluid properties..... 16

Table 2.6 Typical composition of geothermal gas..... 18

Table 2.7 Advantages and disadvantages of the different types of electrolysers..... 25

Table 3.1 Advantages and disadvantages of the heat exchanger types..... 30

Table 3.2 Modelling parameters of intergrated system..... 32

Table 3.3 The reference specific enthalpy and entropy values at 298.15 K and 101.325 kPa 40

Table 3.4 Chemical exergy values of species at 298.15 K and 101.325 kPa..... .41

Table 3.5 Control volume and exergy balance equations of all components..... .43

Table 4.1 Correlations of the cost for the components ..... .47

Table 5.1 Components purchase cost calculations..... .58

Table 5.2 Comparison of LCOM values of this study with those founded in the literature..... 59

CHAPTER ONE
INTRODUCTION

1.1 Introduction

The need for energy in the world and our country is rising daily with the growing industry, population, and the recently accelerated electric vehicle transformation. According to The Energy Institute (EI) report, energy consumption worldwide in 2023 was 620EJ, while global electricity generation increased by 2.5% to a record 29,925 TWh. While fossil fuels are the most widely used source of electricity generation with 60%, the share of electricity generated from renewable sources is 30% (Davenport et al., 2023).

Renewable energy-generating structures have gained importance, especially in recent years, for countries with insufficient fossil fuel resources such as Türkiye. In Türkiye, 45,7% of the energy needed in 2024 was obtained from renewable sources, while 59% of the installed capacity was composed of renewable energy systems (Shura 2024). While increasing energy demand necessitates the development of different systems, the importance of geothermal energy systems, which have been utilized by humanity for many years, is increasing day by day. Türkiye is one of the leading countries in the world in terms of geothermal resources. In fact, Türkiye ranks first in Europe and fourth in the world in electricity generation from geothermal energy. In 2024, according to the Energy Institute's report, Türkiye continues to produce with a capacity of 1.7GWe and 63 licensed plants (Davenport et al., 2023).

Geothermal energy systems differ from other renewable energy systems due to their energy source. As one of the 2050 European Green Deal decarbonization targets, geothermal systems operating with zero carbon emissions are still an important research topic (Fetting, 2020). In a recent study, geothermal systems saved 107 million tons of CO_2 emissions annually (Lund et al., 2011). However, geothermal systems can cause emission pollution with noise, environmental thermal effects, pollution and gas mixture to the atmosphere (Kristmannsdóttir et al., 2003).

1.2 Motivation

This thesis focuses on the system that will reduce the carbon emissions of geothermal energy systems. As an output of geothermal energy systems, there is a gas mixture given to the atmosphere. This mixture contains gases such as CO_2, H_2S, NH_3, N_2, H_2 and CH_4. These gases are known as non-condensable gases because they can not vaporize. These gases are also present in a certain amount in the fluid taken from the production well. In this study, the stages of collecting CO_2 gas, which is discharged into the air and has detrimental effects on nature, instead of being emitted to the atmosphere, then converting it into CH_4 gas by Sabatier reaction are examined. Geothermal energy systems have long been considered a sustainable source of base-load power; however, their environmental impact—particularly the release of non-condensable gases such as CO_2—remains challenging. As global attention shifts toward carbon-neutral and closed-loop energy solutions, integrating synthetic fuel production into geothermal systems offers a promising pathway to enhance environmental and energy performance. Although various studies have analyzed geothermal-based power cycles and renewable fuel production separately, there exists a gap in the current literature regarding the integration of a synthetic methane (CH_4) production unit using 0-dimensional Sabatier reaction kinetics within a geothermal power plant. The lack of techno-economic evaluations for such integrated systems limits their practical applicability. Addressing this gap is critical for developing more efficient, sustainable, and economically viable renewable energy systems.

1.3 Objective

The main aim of this thesis is to analyze a system that produces synthetic methane and does so with a system that can effectively and efficiently use geothermal resources. For this purpose, a geothermal energy system using the Organic Rankine Cycle (ORC) integrated with a proton exchange membrane (PEM) electrolyser and Sabatier reactor is integrated into this system to produce CH_4. Another objective of the thesis is to examine the effects of different gases used in ORC on system efficiency. In order to examine the effect of different ORC fluids on system efficiency, a parametric study was carried out with a code created in the EES program. Another aim of the study is to examine the technical feasibility and economic viability of the system formed by

techno-economic analysis. For this purpose, the necessary literature and sectoral research were conducted, and the results are presented in the following stages of the study.

1.4 Thesis Outline

In the Second Section, renewable energy systems, especially organic rankine cycle systems, and the working principle of the organic rankine cycle are explained together with a literature review. Information about non-condensable gases given to the atmosphere as an output of geothermal energy systems is also given. In addition, information about electrolysers is provided, but PEM-type electrolysers are explained in more detail. A literature review on how synthetic fuel production can be done, Sabatier reactors, and their usage areas are also reviewed and detailed in this section. Finally, information on CO_2 capture systems is also provided.

The Third Chapter includes the description and modeling of the system created within the scope of the thesis, the geothermal system used, the 0-dimensional numerical equation used in the Sabatier reactor, and the parameters of the electrolyser used in the study. Firstly, detailed information about the system for the geothermal system operating with the organic rankine cycle principle and the components used is given. How the CO_2 required for synthetic methane production is obtained from the geothermal system, and the CO_2 capture mechanism is introduced. Afterwards, Sabatier reactors' working principles, usage areas, and outputs were detailed. In the next stage, the operating parameters and numerical equations of the PEM electrolyser used in the study are detailed.

In the Fourth Section, the outputs and efficiency of the system detailed in the previous section are described. Here, the amount of methanol obtained and total system efficiencies according to the type of organic fluid used in ORC and varying reservoir fluid temperatures are specified. In order to obtain the mentioned results, a parametric study was carried out in the EES program and outputs were obtained.

The Final Chapter discusses the conclusions derived from this thesis.

CHAPTER TWO
BACKGROUND AND LITERATURE REVIEW

2.1 Introduction

This section of the thesis provides a general overview of renewable energy systems, including solar, wind, and hydroelectric power, followed by a more detailed examination of geothermal energy systems based on findings from the literature. The working principles and classifications of geothermal energy systems are discussed, with particular emphasis on the Organic Rankine Cycle. Furthermore, electrolysers and their various types are introduced, with a detailed focus on Proton Exchange Membrane (PEM) electrolysers. The Sabatier reaction, which enables the methanation process and represents a key component of this study, is also examined. Additionally, a detailed review of recent literature on Sabatier reactors and the methanation reaction is provided.

2.2 Renewable Energy

In recent years, research conducted by various institutions and their findings have revealed that the climate change crisis is growing day by day. The World Meteorological Organization (WMO) published a report titled State of Global Climate Report 2024, which showed that 2023 was the hottest year on record, with global temperatures rising to an average of 1.5°C. Additionally, according to Cattiaux et al (2024), global daily temperature averages in 2023 reached record levels historically. The significance of renewable resources lies in their ability to help prevent or reduce the impacts of the escalating climate emergency. Furthermore, increasing the use of renewable energy sources is essential to reduce carbon emissions and ensure a sustainable future (Mathiesen et al., 2012; Owusu et al., 2016).

Derived from sustainable sources such as solar, wind, and geothermal, renewable energy represents an inexhaustible form of power. It serves diverse applications, ranging from electricity generation to heating, cooling, and transportation. Additionally, renewable energy sources are an important factor in reducing countries' dependence on foreign energy (Katterbauer et al., 2025). Renewable energy systems

are recognized as alternative and environmentally friendly sources to fossil fuels such as coal, natural gas, and oil (Zycher, B. 2024).

According to a report published by the Energy Institute (EI) in 2024, global energy consumption amounted to 620 EJ, with nearly 30% of this energy coming from renewable sources. 14.2% of this energy was produced by hydroelectric power plants, while 15.9% was produced by other renewable energy sources

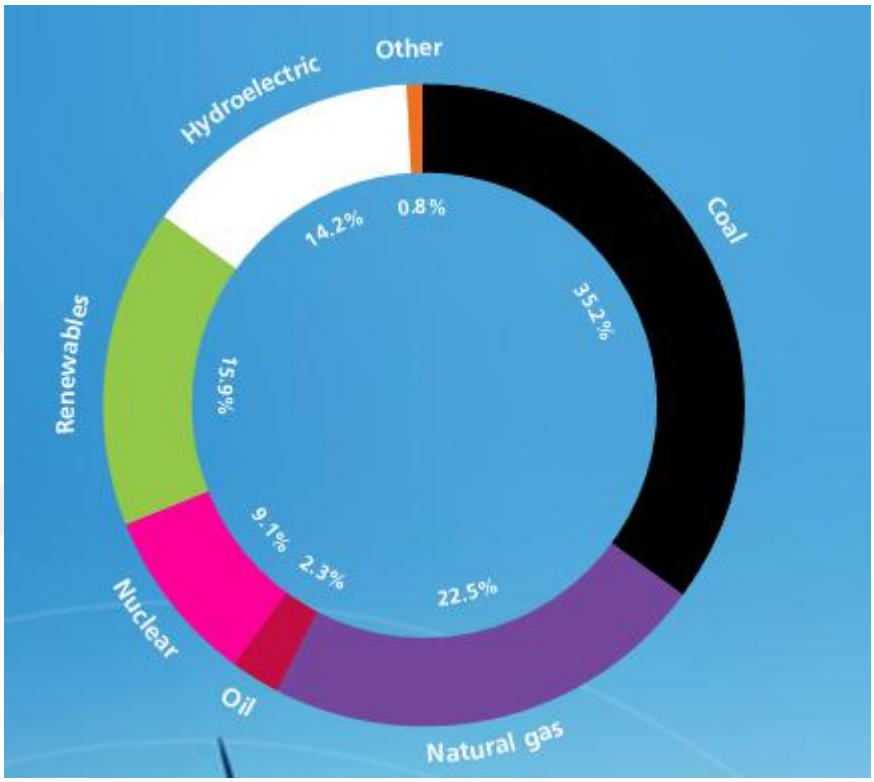

Figure 2.1 Renewable energy production of the different types of plants (Davenport et al., 2023).

Geothermal energy systems occupy a significant place among renewable energy systems. Geothermal resources represent a renewable form of energy capable of contributing to the move toward clean and sustainable energy solutions. However, despite this great potential, geothermal energy systems account for only 0.34% of global energy production, rising from 9,791 MWe in 2009 to 16,316 MWe in 2023 (Nkinyam et al., 2025).

2.2.1 Geothermal Energy

Geothermal energy is the heat energy found in the Earth's core, which can be converted into electrical energy using engineering systems or used directly as hot water or steam (Axelsson, 2024). Geothermal energy provides a consistent and environmentally friendly power supply, making it suitable for continuous use throughout the day and the year. Geothermal projects harness the Earth's thermal energy and make it directly usable for residential or industrial heating applications and electricity generation (Brinkmann, 2023). The Earth's inner core temperature is 6,000 °C and 3,000 °C, which is comparable to the surface of the sun (Hernlund et al., 2008). It is estimated that the massive thermal energy of approximately 42 million megawatts emanating from the Earth's crust will continue to exist for billions of years (Omenikolo et al., 2020).

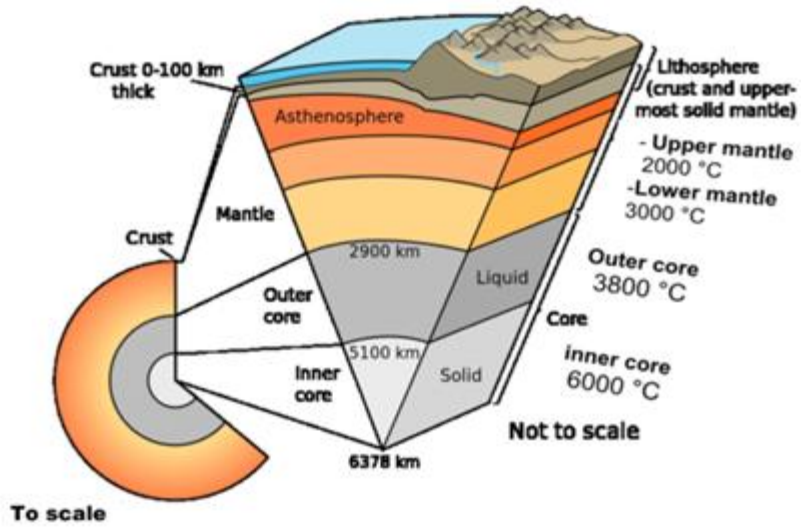

Figure 2.2 Geothermal gradient and Earth’s ınterior layers (Hassan, 2022).

Table 2.1 Evolution of the geothermal power usage (Hassan, 2022)

Date	Location	Description
10,000 years ago	North America	Hot springs used for cooking, bathing
1827	near Pisa, Italy	Industrial boric acid extraction
1892	Idaho, USA	First district heating system
1904	Tuscany, Italy	First geothermal power test
1913	Larderello, Italy	First commercial power plant
1922	USA	First US geothermal plant
1959	California	35 kW experimental station
1960	Larderello, Italy	Multiple plants, 127,650 kW capacity
1946	Portland, Oregon	First ground source heat pump
1958	New Zealand	Wairakei geothermal plant started
1959	Pathe, Mexico	Experimental plant, 588 MW capacity
1960's	USA	First large-scale plant, 11 MW
1966	Japan, Matsukawa	23 MW geothermal plant
1967	Petropavlovsk, Russia	First binary plant, 670 kW
1973	Fenton Hill, NM	Hot-dry-rock (HDR) power generation
1973		Geothermal heat pumps gained use
1980's		Recognized as clean energy source
2000's		Widely adopted, sustainable power
2021		32 countries, increased capacity

Similar to other renewable energy sources, geothermal systems exhibit both advantages and limitations. They are widely regarded as one of the cleanest large-scale energy options currently available. In line with the growing global commitment to reducing atmospheric emissions, technological advancements in geothermal energy have played a substantial role in supporting these efforts. Moreover, potentially harmful constituents present in geothermal fluids are commonly reinjected into the

original reservoir, thereby minimizing their environmental impact and ensuring the system's sustainability. Compared to other energy sources such as oil, gas, and coal, geothermal energy systems require significantly less land for transmission pipelines and power plants (Kabeyi, 2019). Additionally, unlike mining-based energy sources such as coal, geothermal energy requires much less land use during production. When considering the land required per megawatt installed capacity, large-scale hydroelectric projects with dams occupy significantly more space than geothermal power facilities (Bagher et al. 2015).

Geothermal energy systems also have some disadvantages. In general, the installation costs of geothermal energy systems are higher than those of traditional heating and cooling systems (Molavi et al., 2016). Environmental impacts may arise in the event of incorrect installation or operation of the systems; for example, land subsidence may occur due to continuous groundwater extraction. A leak in the pipes could pose a risk of contamination to the environment and groundwater (El Shinawi et al., 2022). There are also some concerns regarding sustainability. In geothermal systems, rainwater that seeps from the surface into the ground replenishes reservoirs; however, if this liquid is extracted faster than it is naturally replenished (aquifer recharge), reservoirs may eventually deplete (Menéndez et al., 2019).

2.2.1.1 Exploring Geothermal Energy's Contribution to Sustainable Power Generation

As global energy demand continues to grow and the impacts of climate change become increasingly severe, geothermal energy systems are attracting greater attention due to their high reliability and low carbon dioxide emissions. Despite their significant advantages and potential, geothermal systems currently contribute less than 1% to global energy demand, according to a report published by the IEE in 2024. However, the report indicates that they could contribute up to 15% of electricity demand by 2050 (Menéndez et al., 2019). According to a report published in December 2022, the installed geothermal energy capacity across 198 locations in 32 different countries worldwide is 16,318 MW (Gutiérrez-Negrín, 2024). This capacity still accounts for only 0.16% of the global installed electricity capacity of 10,216,390 MW in 2022. Over the years, the number of geothermal plants has increased with investments made

by countries around the world. The following table illustrates the progression of geothermal energy systems from 1980 to 2023.

Table 2.2 Evolution of geothermal power worldwide in the last 43 years. (Gutiérrez-Negrín., 2024)

Years	**Capacity (MW)**	**Capacity Factor (%)**	**Generation (GWh)**			**Share of (%)**	
			Geothermal	Clean energy	Total	Clean energy	Total
1980	2110	70.87	13.1	2.438.000	5.633.000	0.54	0.23
1985	4764	69.32	28.93	3.547.900	9.831.380	0.82	0.29
1990	5834	69.33	35.43	4.351.600	11.853.110	0.81	0.30
1995	6832	63.55	38.035	5.022.400	13.382.480	0.76	0.28
2000	7972	70.54	49.261	5.485.400	14.971.790	0.90	0.33
2005	8933	71.19	55.709	6.044.100	17.678.940	0.92	0.31
2010	10.897	70.45	67.246	6.958.800	20.938.060	0.97	0.32
2015	12.284	68.35	73.55	8.142.800	23.660.330	0.90	0.31
2020	15.414	66.35	89.587	10.186.500	26.276.910	0.88	0.34
2023	16.318	67.54	96.552	11.143.100	28.254.250	0.87	0.34

Electricity is actively generated using geothermal energy systems in 32 countries around the world. Although these systems are actively used in many countries, there are countries referred to as the 1 GW club, which are the United States, Indonesia, the Philippines, Türkiye, and New Zealand. Kenya is the country closest to joining this club, with a capacity of 985 MW. Hutter (2020), published a report in 2020 detailing the installed geothermal capacity and electricity production of countries in 2018 and 2019. Similar studies were conducted in 2021 and 2022, and the results are presented in the table below.

Table 2.3 Recent trends in installed capacity and energy production from geothermal sources. (Gutiérrez-Negrín., 2024)

		2018-2019		2021-2022		Net changes in:
Country	**Capacity (MW)**	**Generation (GWh)**	**Capacity (MW)**	**Generation (GWh)**	**Capacity (MW)**	**Generation (GWh)**
Australia	0.3	1.7	0.3	0	0	-1.7
Austria	1.2	2.2	0.3	0.5	-0.9	-1.7
Belgium	0	0	0	0	0	0
Canada	0	0	0	0	0	0
Chile	48	400	81	600	33	200
China	29.1	174.6	45.1	131.2	16	-43.4
Colombia	0.1	0.1	0	0	0	0
Costa Rica	207	960	252.5	1,599	45.5	639
Croatia	16.5	764	16.5	747	0	-17
El Salvador	204.4	1,440.2	204.4	1,575	0	133
Ethiopia	7.3	136	7.3	127	0	-9
France	7	136	7	127	0	-9
Germany	46.1	165.6	46	207.7	-0.1	42.1
Guatemala	52	237	46.5	310	-5.5	73
Honduras	35	270	35	297	0	27
Hungary	3	27	3	27	0	0
Iceland	755	6,010	755.4	5,788.4	0.4	-221.6
Indonesia	1,955	15,131	2,583.4	16,588.2	628.4	457.2
Italy	915.5	6,015	915.5	5,917	0	-98
Japan	619	2,501	619	2,500	0	-1
Kenya	865.4	5,240	972.5	5,590	107.1	350
Mexico	1005	5,200	1,021.7	5,210	16.7	10
New Zealand	1,054.8	7,564	1,054.6	7,820	-0.2	256
Nicaragua	155	804	195	1,092	40	288
Philippines	1918	9,893	1,951.8	11,670	33.8	1,777
Portugal	33	216	33	211	0	-5.1
Romania	0	0	0.8	0.5	0.8	0.5
Russia	23	4407	23	4,427	0	20
Taiwan	0.3	2.6	0.6	4.8	0.3	2.2
Thailand	0.1	2	0.2	0.6	0.1	-1.4
Türkiye	1,549	8,168	1,717.3	10,440	168.3	2,272
United States	3,678.2	18,435	3,919.4	2,412.2	241.2	2,627.2
Total	15,413.5	89,586.9	16,318.4	96,552.1	904.9	6,965.2

Accordingly, the United States ranks first in the world in this field with a geothermal capacity of 3919.4 MW. Indonesia ranks second with 2384.4 MW, while the Philippines ranks third with 1951.8 MW. Türkiye ranks fourth on the list with

1,717.3 MW, following the Philippines. Similar to global trends, investments in geothermal energy are steadily increasing in our country. According to a recent study completed at the end of 2024, Türkiye's installed geothermal capacity has reached 1,734 MW (Cariaga et al., 2025).

The European Geothermal Energy Council (EGEC) predicts that the growth momentum of geothermal energy in Europe will increase in 2025 and beyond. Their 2024 report states that two new geothermal power plants have recently become operational in Türkiye, with one more in Austria. Additionally, around 50 new geothermal power projects and over 500 geothermal heating and cooling systems are currently in development (EGEC, 2025). Geothermal energy systems can be used not only for electricity generation but also for heating in residential buildings. Therefore, the European Union has proposed the idea of preparing a new European Geothermal Action Plan to maximize the efficiency of geothermal systems. It has also called for an increase in internal capacity in this area and easier access to financing (Geothermal energy,2024) In addition to the EGEC, the IOGP and Europe have jointly published a statement indicating that by 2030, approximately 25% of residential heating and 10% of total energy needs could be met by geothermal systems (IOGP Europe, 2025). "As project costs continue to decline and technological advancements emerge over the next few years, geothermal energy could potentially supply up to 15% of the world's electricity demand by 2050. This would mean that geothermal energy systems would reach a capacity of 800 GW worldwide by 2050 (IEA 2024).

2.2.1.2 Working Principle and System Types of Geothermal Systems

Geothermal energy is a renewable and sustainable mechanism that utilizes engineering systems to extract heat accumulated in the Earth's crust and use it for heating, industrial applications, and most commonly, electricity generation. This section will detail the operating principle of geothermal energy systems. Geothermal systems are engineering systems that use carrier fluids such as water or steam to extract heat from the Earth's crust and convert it into electricity using specialized systems.

The first geothermal system was experimentally established by Italian scientist Piero Ginori Conti in 1903, who succeeded in operating a generator. The first

commercial-scale geothermal energy plant was commissioned in Larderello, Italy, in 1913 (Parri et al., 2016). With the advancement of technology and increasing knowledge, many different geothermal systems have emerged today. In this context, various kinds of systems have emerged, such as direct steam, binary cycle, and flash steam systems, each with advantages and limitations. The most essential factors in selecting a system to be installed in a region are reservoir temperature, pressure, fluid properties, and, of course, geological structure. The most commonly used geothermal systems in industry are known as dry steam, flash steam, and binary cycle systems (Lee, 2001). The most crucial limitation in selecting which of these systems to use is the reservoir temperature. Accordingly, in reservoir temperature-based classification, low-enthalpy systems are defined as those below 90°C, medium-enthalpy systems as those between 90°C and 150°C, and high-enthalpy systems as those above 150°C.

Table 2.4 shows the classification of geothermal reservoirs and provides some examples of these reservoirs. Reservoirs in the low enthalpy class are used for heating rather than energy production, while reservoirs in the medium and high enthalpy classes are used for electricity production. Accordingly, the reservoir located in Balçova, Izmir, belongs to the low-enthalpy class and is used for heating in homes, while the facility in Kızıldere, Denizli, operates as an electricity-generating facility using a reservoir belonging to the high-enthalpy class.

In addition to enthalpy-based classifications, Lee (2001) proposed an exergy-based indicator known as the Specific Exergy Index (SExI) to assess the thermodynamic quality of geothermal resources. Unlike temperature or enthalpy alone, this index considers the potential of geothermal fluids to perform useful work relative to environmental (reference) conditions. SExI is defined as:

$$SExI = \frac{h - T_{ref} \cdot s}{h_{max}} \qquad 2.1$$

where h is the specific enthalpy, s is the specific entropy, and T_{ref} is the reference temperature. Based on SExI values, geothermal resources can be classified as: low, medium and high quality. According to Lee's classification, geothermal fluids with a SExI value below 0.05 are considered low quality, indicating minimal potential for power generation and better suitability for direct-use applications. Fluids with SExI

values between 0.05 and 0.5 are categorized as medium quality, suggesting they may be viable for direct use and power production through systems like binary cycles. Lastly, resources with a SExI of 0.5 or higher are classified as high quality, making them ideal candidates for efficient electricity generation using technologies such as flash or dry steam systems. (Lee, 2001)

Table 2.4 Classification of the geothermal reservoir (Hossain et al. 2021; Lee, 2001)

Category	**Temperature (°C)**	**Description and Applications**	**Example Reservoirs (Country)**	**Specific Exergy Index (SExI) Range**
Low Enthalpy	20 - 90°C	These resources are ideal for direct use applications like spa tourism, greenhouse heating, aquaculture, and residential heating	Baden-Baden (Germany), Paris Basin (France), Balçova (Türkiye)	SExI < 0.05
Medium Enthalpy	90 - 150°C	These fields can be used for both direct applications and electricity generation.	Geothermic Val d'Agri (Italy), Tuzla (Türkiye)	0.05 ≤ SExI < 0.5
High Enthalpy	150°C and above	These high-temperature fields are the most efficient for electricity generation.	The Geysers (USA), Larderello (Italy), Kızıldere (Türkiye), Hellisheiði (Iceland)	SExI ≥ 0.5

Dry steam power plants are the oldest and most basic geothermal system structures. Steam at a temperature of 150 °C or higher taken from the reservoir directly drives the generators, thereby producing electrical energy (Fridleifsson et al., 2008). No organic fluid is used in these systems; pipes are installed to directly convey the fluid from the reservoir to the generator. Two types of turbines are used in dry steam power plant systems: backpressure or condensing turbines. In back-pressure turbines, the steam passes through the turbine and is released into the atmosphere (Kabeyi et al., 2021). This type of turbine is suitable for situations where the non-condensable gas content in the steam is 12% or higher (Bowen, 2012). In condensing turbines, the steam exiting the turbine is condensed and returned to the reservoir.

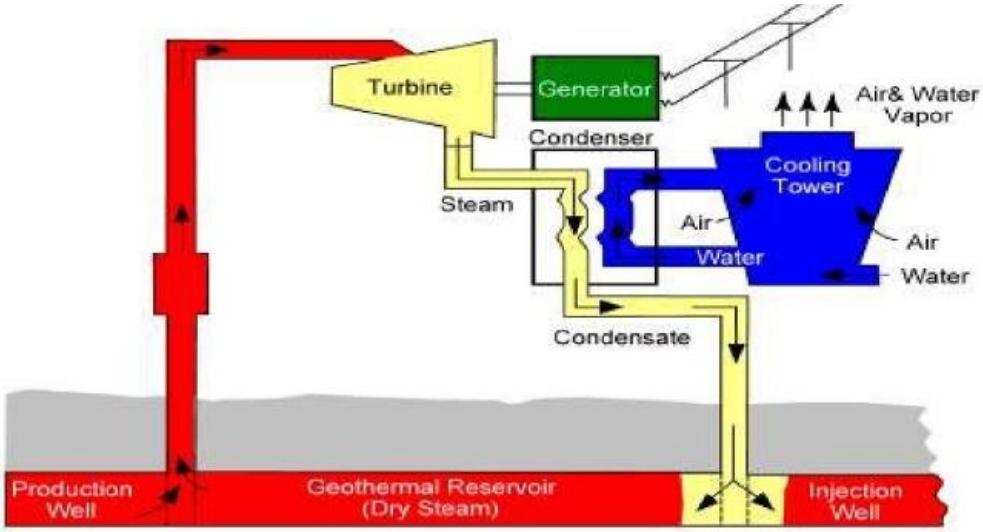

Figure 2.3 Dry steam geothermal power plants (Ikechukwu, 2021)

Flash Steam Geothermal Power Plants are systems that suddenly reduce the pressure of high-pressure liquid with a reservoir temperature of 180 °C or above, convert it into steam, and then send the steam to the turbine. The steam exiting the turbine is then condensed and reinjected into the reservoir to maintain reservoir health and continuity (Dagdas, 2007; Kaya et al., 2011). The sudden reduction in fluid pressure from the reservoir causes part of the fluid to vaporize instantly, a process known as flashing. Even when the fluid pressure from the reservoirs of power plants using this type of system is reduced and converted into steam, it remains at a high enough pressure to turn the turbine and thus generate electrical energy (Aliyu et al., 2019). There are two basic types of flash steam systems: single flash and double flash. In single-flash steam systems, the geothermal fluid is converted into pressurized steam through a single-stage pressure reduction and sent to the turbine. In contrast, in double flash systems, the pressure reduction occurs in two stages, resulting in an additional 15%-25% increase in electricity production.

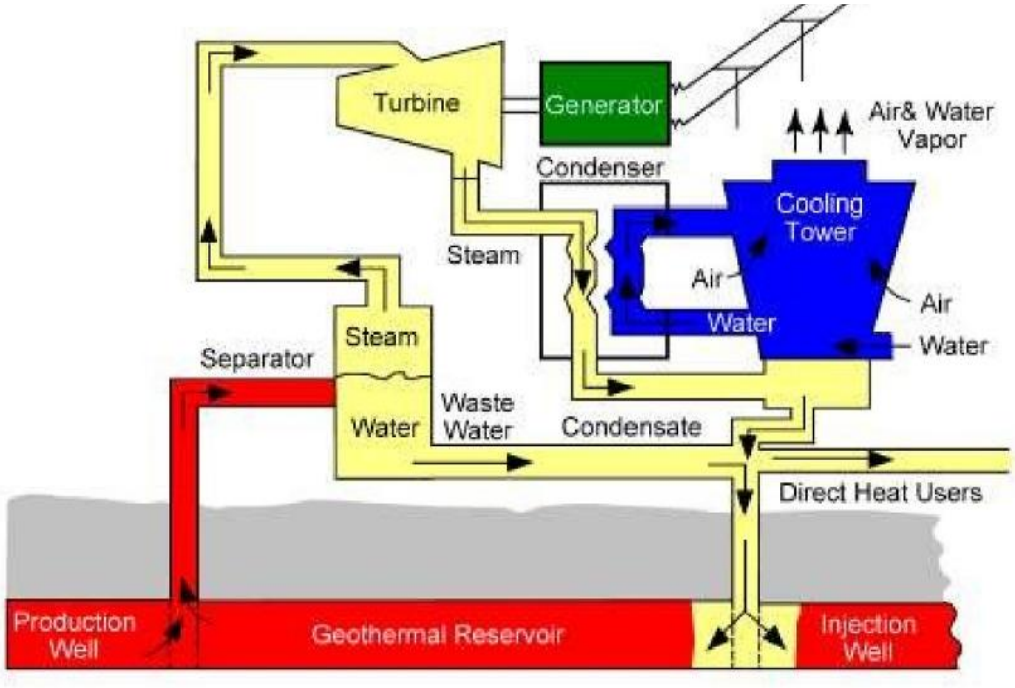

Figure 2.4 Flash steam geothermal power plants (Ikechukwu, 2021)

Binary power plants are used in locations where the reservoir temperature is between 107°C and 182°C (Ikechukwu, 2021). The main difference between these systems and dry and flash power plants is that the fluid taken from the reservoir is not used directly, but as a secondary fluid. Here, the heat of the fluid taken from the reservoir is transferred to the working fluid to be used in the turbine via a heat exchanger (Hossain et al., 2021). In this system, the fluid taken from the reservoir is called the primary fluid, and the secondary fluid, i.e., the fluid sent to the turbine, is an organic fluid (Kabeyi et al., 2019). The secondary fluid absorbs heat from the primary fluid and, due to its much lower boiling point, easily transitions to the vapor phase at high pressure, after which it is sent to the turbine and electricity is generated by the generator. The main advantage of this cycle is that it operates at low temperatures due to the very low boiling point of the secondary fluid, and since there are two separate closed circuits, no harmful elements are released into the atmosphere or the environment (Alam et al., 2025). This type of geothermal energy system varies depending on the type of secondary fluid sent to the turbine (Kabeyi et al. 2019) (Chowdhury et al. 2023). These can be categorized as ORC, Kalina, and Goswami.

ORC-type systems use fluids such as R-134a, R141b, n-pentane, and n-butane as the secondary fluid, while Kalina and Goswami systems use ammonia.

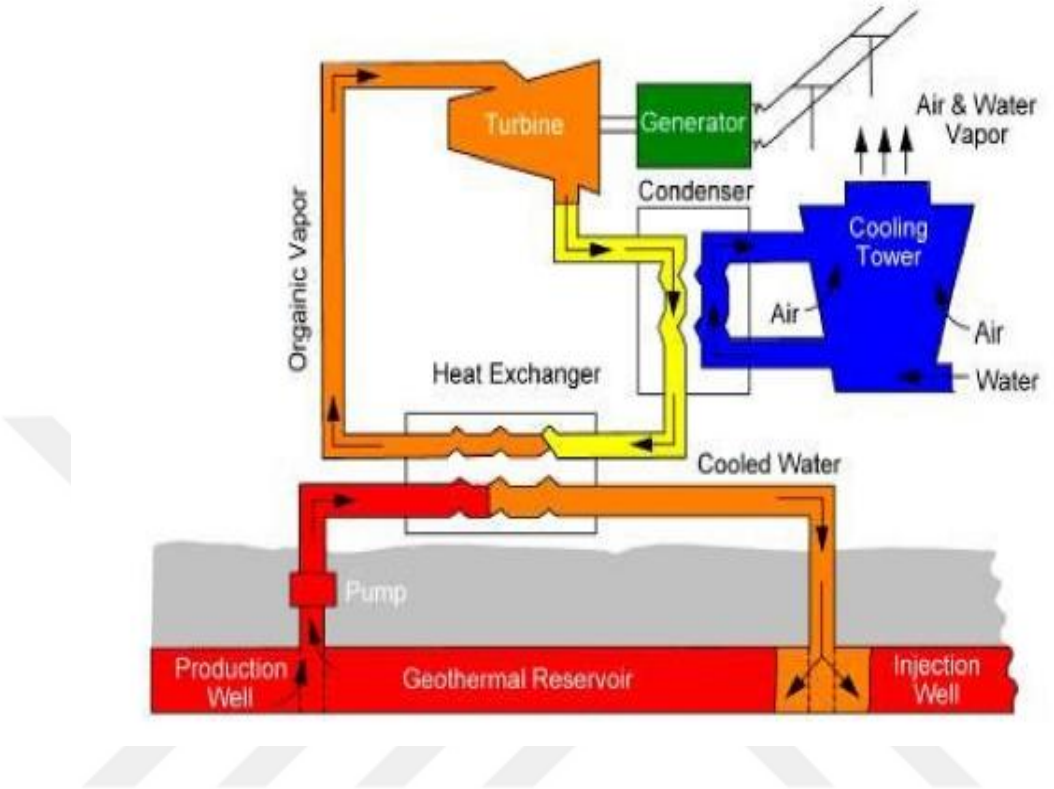

Figure 2.5 Binary geothermal power plants (Ikechukwu., 2021)

The following table lists the fluids commonly used in organic Rankine cycles.

Table 2.5. Different ORC working fluid properties (Liang et al., 2019)

Working Fluid	Typical Temperature Range (°C)	Environmental and Operational Characteristics	GWP/ODP/ASHRAE 34 Safety Class
R245fa (HFC)	100–150	Low GWP, non-toxic, non-flammable; high efficiency at low temperatures	1030-0-A1(non-flammable, low toxicity)
n-Pentane (Hydrocarbon)	~120	High thermal efficiency, low critical pressure advantage; good performance in supercritical use.	~4 / 0 / A3
Toluene (Aromatic)	250–300	Highest efficiency; flammable and environmental risks	~3 / 0 / A3
HFE7100, HFE7000 (Fluorinated Ethers)	–	Low environmental impact, safe to use; environmental and safety advantages	297-322 / 0 / A1

Table 2.5 Continued			
n-Decane	–	High cycle efficiency but requires large equipment (due to high vapor volume).	~4 / 0 / A3
R1234ze(E) (HFO)	–	Low GWP next-generation fluids, considered as alternatives to R245fa	<1 / 0 / A2L
n-Butane (Hydrocarbon)	80–120	Low GWP, high cycle efficiency; suitable for low-temperature geothermal and waste heat recovery; flammable	~4 / 0 / A3
R143a (HFC)	120–170	Low to moderate GWP, non-flammable; moderate ODP; used in medium temperature ORC applications.	4470 / 0 / A1
R141b (HCFC)	140–180	Non-flammable, moderate GWP, moderate ODP; usage limited due to ozone depletion potential.	700-2500 / ~0.12 / A1
Ethanol, Methanol, Propanone	150–200	Potential working fluids in ORC; thermodynamic performance and economic analyses available.	~0 / 0 / A3

Table 2.5 shows various characteristics of different working fluids, including their operating temperature ranges, environmental and operational impacts, Global Warming Potential (GWP), Ozone Depletion Potential (ODP), and ASHRAE Standard 34 safety classifications. In this classification system, the A1 safety class indicates non-flammability and low toxicity, A2L denotes mildly flammable substances with low flame propagation, and A3 refers to substances that are highly flammable.

2.3 Non-Condensable Gases

In geothermal systems, gases are carried along with steam from the reservoir during production but do not condense when cooled. These are called non-condensable gases (NCGs). These gases are typically carbon dioxide (CO_2), hydrogen sulfide (H_2S), methane, and nitrogen. However, the proportions of these gases vary depending on the location and source of the geothermal system (Li et al., 2022). The presence of non-condensable gases in the steam negatively affects the vacuum process in the condenser, increases turbine back pressure, and reduces the efficiency of the energy production process (Sufyana et al., 2023). Therefore, to optimize the thermodynamic efficiency

of a geothermal power plant, NCGs must be removed using a gas removal system. Since CO_2 and H_2S, the two most abundant gases in a geothermal fluid, are acidic and can have a negative effect on equipment, they must either be released into the atmosphere using NCG removal systems or returned to the reservoir.

CO_2 gas has the highest concentration among non-condensable gases, ranging from 75% to 99%. The second most abundant gas is H_2S, ranging from 0.1% to 21.2%. A common compositional range of geothermal gases is shown in Table 2.7.

Table 2.6 Typical composition of geothermal gas (Fridriksson et al., 2016)

	Median (wt% dry gas)	**Maximum (wt% dry gas)**	**Minimum (wt% dry gas)**
CO_2	95.4	99.8	75.7
H_2S	3.00	21.20	0.10
H_2	0.01	2.20	0.00
CH_4	0.15	1.70	0.00
NH_3	0.29	1.80	0.01
N_2	0.84	3.00	0.17
Ar	0.02	0.04	0.00

If the gas is not injected into the reservoir and H_2S gas does not exceed environmental standards, these gases are released into the atmosphere. Systems that capture non-condensable gases can be used to reduce environmental damage and carbon footprint. The majority of NCG gases are CO_2 gases. Figure 2.9 shows a schematic diagram of an NCG ventilation system integrated into a flash steam power plant.

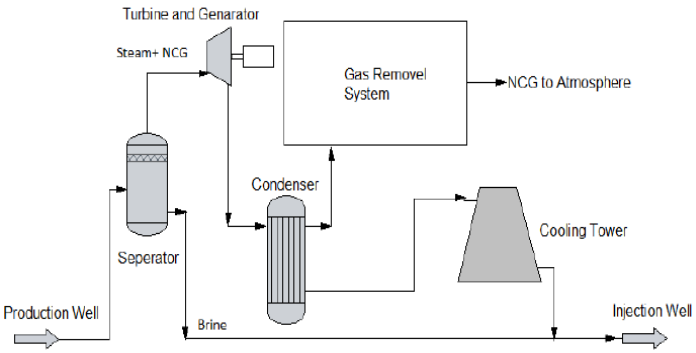

Figure 2.9 An NCG system integrated into a flash steam power plant (Aksoy et al. 2015)

2.4 Sabatier Reaction

The problem of climate change is growing day by day. Carbon dioxide (CO_2) is one of the most important greenhouse gases in the atmosphere. In particular, the concentration of CO_2 in the atmosphere has increased significantly in recent years as a result of growing industrial activity. Burning forests, the daily increase in the number of fossil fuel-powered vehicles, and the growth and expansion of industrial facilities are the main factors contributing to the rise in CO_2 emissions (Herath et al., 2020). Preventing the greenhouse effect caused by CO_2 emissions into the atmosphere plays a major role in solving this problem, and this is where the Sabatier reaction comes into play.

The Sabatier reaction is an exothermic reaction in which carbon CO_2 and hydrogen gas (H_2) are reacted to produce CH_4 and H_2O. Using CO_2 in the Sabatier reaction is an important part of environmental health, sustainable energy production, and carbon capture technologies. Sabatier reactions enable the controlled production of synthetic methane using hydrogen and carbon dioxide and are widely used, particularly in the production of synthetic methane using renewable hydrogen (Wisniak, J., 2005). The Sabatier reaction used in synthetic methane production is shown Equation 2.2.

$$CO_2 + 4H_2 \leftrightarrow CH_4 + 2H_2O \qquad \Delta H^{298K} = -164.9\ kJ/mol \qquad 2.2$$

In Sabatier reactors, CO_2 methanation can also occur alongside the exothermic Sabatier reaction, through reverse water-gas shift (RWGS) and exothermic CO methanation reactions, which are described in Equations 2.3 and 2.4, respectively (Herath et al., 2020).

$$CO_2 + H_2 \leftrightarrow CO + H_2O \quad \Delta H^{298K} = 41\ kJ/mol \qquad 2.3$$

$$CO + 3H_2 \leftrightarrow CH_4 + H_2O \quad \Delta H^{298K} = -206.1\ kJ/mol \qquad 2.4$$

Thermodynamic studies in the literature show that when the reaction temperature exceeds 600°C, RWGS and CO methanation become more dominant. Additionally, it is known that a H_2/ CO_2 ratio of less than 4 causes carbon deposition (Molino, 2015; Swapnesh, 2014). At low reaction temperatures of 220-300°C and high H_2/ CO_2 ratios

of 4 and 5, the methanation reaction can be completed via the Sabatier reaction shown in Equation 2 (Herath et al., 2020).

Since the Sabatier reaction is an exothermic reaction, it is carried out with the help of catalysts that can provide high conversion efficiency even at low temperatures. The choice of catalyst in the Sabatier reaction is of vital importance as it directly affects the system's efficiency, continuity, and methane selectivity (Vogt et al., 2019). The most commonly used catalysts are nickel (Ni)-based catalysts, due to their relatively low cost and high methane selectivity. Nickel catalysts begin to sinter at high operating temperatures, which negatively affects the catalyst's active surface area (Xing et al., 2025). To prevent this and maintain the system's sustainability, different support materials (Al_2O_3, SiO_2, TiO_2, ZrO_2, CeO_2) are used.

2.5 Electrolyser

Fossil fuels are still the most widely used source of energy production, and as a result, global warming and environmental pollution problems are growing day by day. Hydrogen, on the other hand, is seen as the fuel of the future, with hydrogen-powered vehicles already in use today. However, producing hydrogen requires its own technology. In particular, when hydrogen is produced without emitting any greenhouse gases, it becomes a much more meaningful fuel, known as green hydrogen. Electrolysers play a crucial role in green hydrogen production, as they help reduce dependence on fossil fuels, lower carbon emissions, and integrate renewable energy sources. Water can be decomposed using direct electric current, and hydrogen and oxygen are produced from water through redox reactions. An electrolyser is the device that combines oxidation and reduction reactions to produce hydrogen and oxygen gas (Zhang et al., 2016). There are three types of electrolytes commonly used in electrolysers: liquid electrolyte, solid polymer electrolyte in the form of a proton-conducting membrane, or oxygen ion conduction membrane (Dincer et al., 2011). Depending on the type of electrolyte used, there are four types of electrolysers: alkaline, anion exchange membrane (AEM), proton exchange membrane or polymer electrolyte membrane (PEM), and solid oxide electrolysers (SOE).

Alkaline electrolysers are an old technology used for hydrogen production in industrial systems with capacities up to multi-megawatts in commercial applications worldwide (Kuckshinrichs et al., 2017). In fact, more than 400 alkaline electrolysers were used in industrial applications as early as the beginning of the 19th century (Grigoriev et al.,). Alkaline electrolysers operate at low temperatures of 30-80 °C using an alkaline solution (KOH/NaOH). Moreover, in alkaline water electrolysers, nickel (Ni)-coated stainless steel electrodes and asbestos/Zr O_2 -based diaphragms are used as a separator (Ramakrishna et al., 2017). An alkaline solution, which is typically 20-40% potassium hydroxide (KOH), is used as the electrolyte to increase ionic conductivity in the cell stack (Ball et al., 2009). Water is reduced at the cathode to generate hydrogen and hydroxide. The hydroxide is circulated through the diaphragm to the anode and recombined to generate oxygen. The reaction kinetics of the alkaline electrolyser are described in Equations 2.5 and 2.6.

$$Anode: \ 2OH^- \rightarrow \frac{1}{2}O_2 + H_2O + 2e^- \qquad 2.5$$

$$Cathode: \ 2H_2O + 2e^- \rightarrow H_2 + 2OH^- \qquad 2.6$$

$$Overall: \ H_2O \rightarrow H_2 + \frac{1}{2}O_2 \qquad 2.7$$

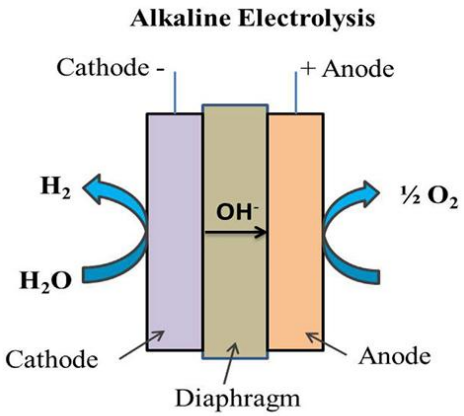

Figure 2.6 Alkaline electrolysers working scheme (Himabindu et al., 2019).

PEM electrolyser was first conceptualized by Grubbs and developed by General Electric in 1966. Typically, PEM electrolysers operate at low temperatures (30–80°C)

and high current densities (1–2 A/cm²) and produce high-purity H_2 and O_2 (Himabindu et al., 2019). PEM electrolysers are safer than alkaline electrolysers because they do not contain caustic electrolytes and have a smaller footprint. The main difference between PEM and alkaline electrolysers is that PEM electrolysers use a solid polymer membrane instead of a liquid electrolyte. In a PEM electrolyser, water is oxidized at the anode to produce oxygen, hydrogen, and electrons. Protons pass through the proton exchange membrane to the cathode, while electrons reach the cathode side via an external circuit. Subsequently, protons are reduced at the cathode, producing hydrogen. The reactions occurring at the anode and cathode are represented by Equation 2.8 and Equation 2.9, respectively.

$$Anode: \quad H_2O \rightarrow \frac{1}{2}O_2 + 2H^+ + 2e^- \qquad 2.8$$

$$Cathode: \quad 2H^+ + 2e^- \rightarrow H_2 \qquad 2.9$$

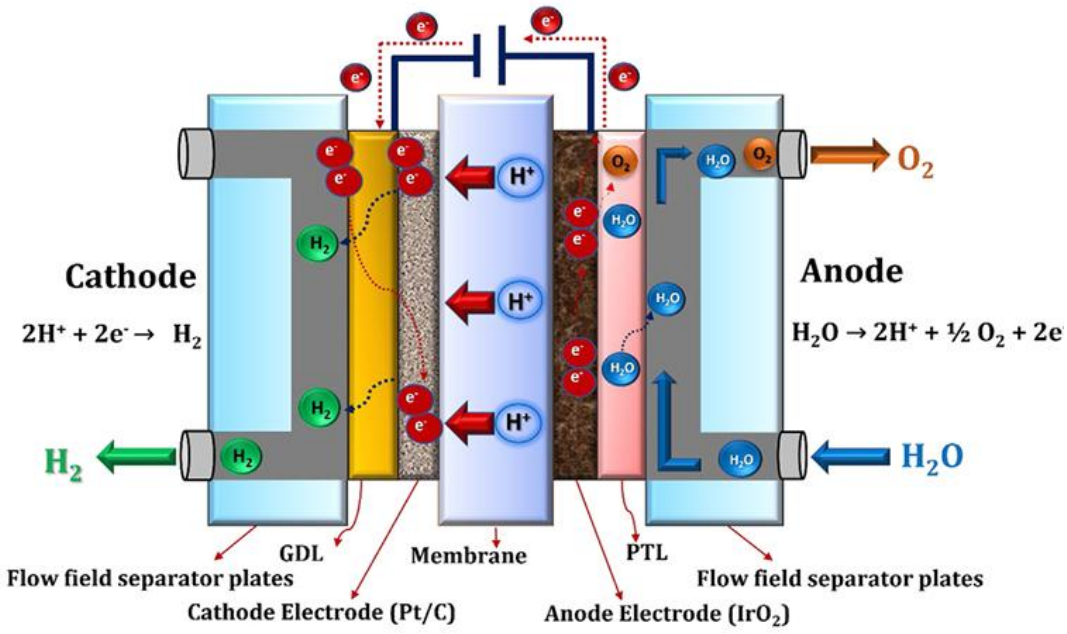

Figure 2.7 PEM electrolyser working scheme (Lim, H., 2022)

Another commonly used type of electrolyser is the solid oxide electrolyser. The solid oxide water electrolysis cell (SOEC) is one of the electrochemical conversion cells, which converts electrical energy into chemical energy (Lim, 2022). Solid Oxide

water electrolysis studies began in the 1970s at General Electric and Brookhaven National Laboratory in the United States and later continued in Germany with Dornier. SOEC electrolysers operate at high temperatures (500-850 °C) with water in vapor form, thereby reducing the power consumption required to separate water into hydrogen and oxygen and ensuring high efficiency. Compared to other types of electrolysers, SOEC electrolysers provide unmatched conversion efficiency due to their method (Khan et al., 2018). In SOEC electrolyzers, two electrons are added to the high-temperature water molecule entering the cathode, thereby reducing it to H_2 and O_2^-. While hydrogen is extracted from the system by the cathode, the O^{2-} ion passes through the membrane to the anode side, releasing electrons and oxygen gas. The following figure shows the operating diagram of an SOEC electrolyser. Equations 2.10 and 2.11 show the reaction equations of the AEM electrolyzer.

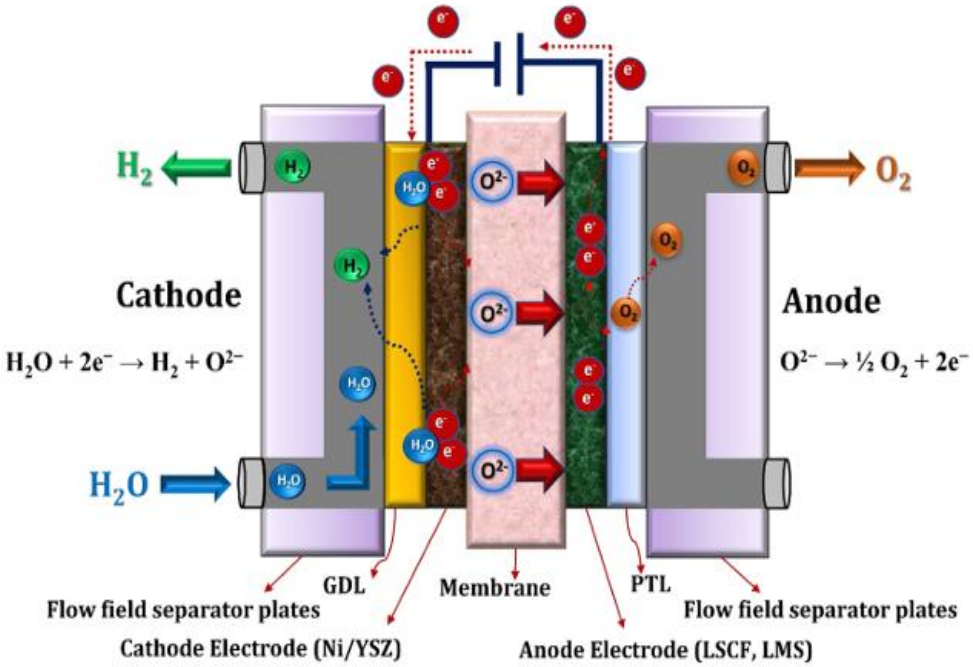

Figure 2.8 Schematic view of solid oxide water electrolysis working principle (Lim, H., 2022)

$$Anode: \ O^{2-} \rightarrow \frac{1}{2} O_2 + 2e^- \qquad 2.10$$

$$Cathode: \ H_2O + 2e^- \rightarrow H_2 + O^{2-} \qquad 2.11$$

SOE is a system that is difficult to integrate with renewable energy sources because fluctuations can occur in the power obtained from renewable energy sources. These fluctuations can cause heat loss and cell temperature loss in SOE, which must operate at high temperatures, and therefore, it is not suitable for use with renewable sources. Such changes cause microcracks in the membrane and significantly reduce the electrolysis's lifespan (Bhandari et al., 2014).

Anion Exchange Membrane (AEM) electrolyzers have recently emerged as a promising water-splitting technology that combines the benefits of conventional alkaline and Proton Exchange Membrane (PEM) electrolyzers. In AEM systems, hydroxide ions (OH^-) move through the anion-selective membrane. This enables hydrogen production using non-precious metal catalysts and less corrosive alkaline electrolytes. This design reduces the overall system cost and improves safety compared to the strongly alkaline solutions used in traditional systems (Xu et al., 2020; Vincent & Bessarabov, 2018). Recent studies show that operating parameters, such as current density, electrolyte concentration, and temperature, significantly affect the efficiency and durability of AEM electrolyzers (Zhang et al., 2023). However, challenges remain with the long-term stability of membranes and ionic conductivity, which currently hinder large-scale commercialization (Vincent & Bessarabov, 2018; Varcoe et al., 2014). Still, ongoing improvements in membrane chemistry and electrode design suggest that AEM electrolyzers could play a key role in future, cost-effective, and sustainable hydrogen production. Equations 2.12 and 2.13 show the reaction equations of the AEM electrolyzer.

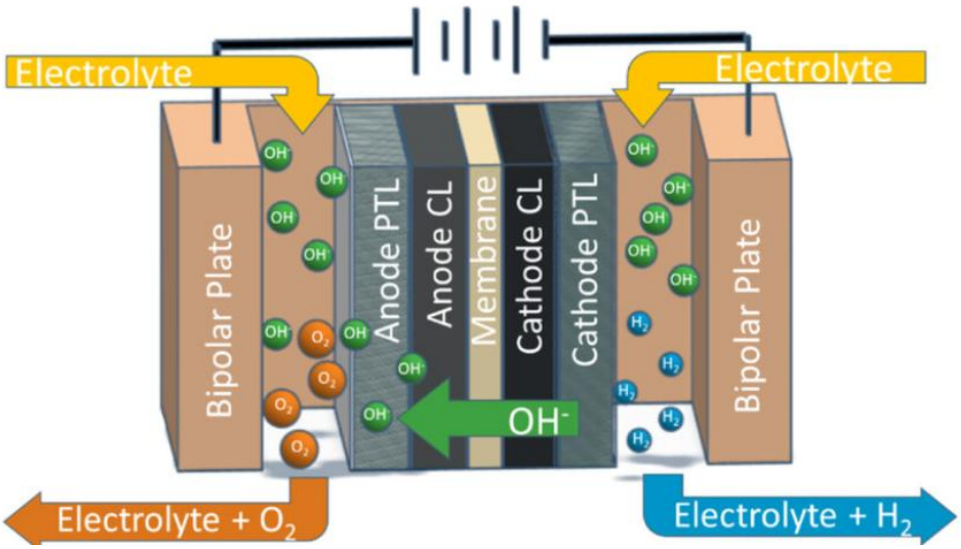

Figure 2.9 Schematic view of the AEM electrolyzers (Liu et al., 2021)

$$Anode:\ 4OH^- \rightarrow O_2 + 4e^- \qquad 2.12$$

$$Cathode:\ 4H_2O + 4e^- \rightarrow 2H_2 + 4OH^- \qquad 2.13$$

Table 2.7 Advantages and disadvantages of the four different electrolyzers (Lim, 2022; Peach, 2022)

Electrolysis process	Advantages	Disadvantages
Alkaline Electrolysis	Well established technology; Non-noble electro catalysts; Low cost technology; The energy efficiency is (70–80%); Commercialized	Low current densities; Formation of carbonates on the electrode decreases the performance of the electrolyser; Low purity of gases;
Solid Oxide Electrolysis	Higher efficiency (90–100%); Non-noble electro catalysts; High working Pressure	Laboratory stage; Large system design; Low durability
PEM Electrolysis	High current densities; Compact system design and Quick Response; Greater hydrogen production rate with High purity of gases (99.99%); Higher energy efficiency (80–90%); High dynamic operation	New and partially established; High cost of components; Acidic environment; Low durability; Commercialization is in near term
AEM Electrolysis	Use of inexpensive catalysts and materials (Ni, Fe, Co instead of Pt/Ir), high efficiency potential, compact and modular design capability.	Membrane durability and longevity are limited, catalyst stability is problematic (corrosion and loss of activity), ion conductivity is lower than PEM low temperature resistance

CHAPTER THREE
MATHEMATICAL MODELLING OF POWER TO SYNTHETIC METHANE PRODUCTION SYSTEM

3.1 Introduction

This chapter discusses the modeling techniques and equations of a system that produces synthetic methane. In this system, power and carbon dioxide are obtained from a geothermal plant, hydrogen is obtained from a proton exchange membrane type electrolyser, and synthetic methane is produced in a Sabatier reactor. This chapter provides an in-depth exposition of the modeling frameworks and equations underlying a synthetic methane production system. In this integrated system, electrical power and carbon dioxide are sourced from a geothermal power plant, hydrogen is produced via a proton exchange membrane (PEM) electrolyzer, and synthetic methane is subsequently synthesized in a Sabatier reactor through catalytic methanation. A detailed analysis of the system architecture, reaction mechanisms, and operational parameters is presented in the following section.

3.2 System Description

The integrated geothermal energy, PEM electrolysers, and Sabatier reactor diagrams are shown in Figure 3.1. As shown in Figure 3.1, the ORC system works as follows. The geothermal fluid obtained from the production well is sent to the heat exchanger, transferring its heat to the ORC working fluid. Here, the organic fluid may be in a critical or supercritical state. The organic fluid is then sent to the turbine, where electricity is generated. After the turbine, the fluid, whose pressure and temperature have decreased, is sent to the regenerator, which is used to increase the system's thermal efficiency. The organic fluid exiting the regenerator enters the air-cooled condenser (ACC) and returns to the heat exchanger, thus completing the cycle. The geothermal fluid is then returned to the injection well to ensure sustainable and renewable energy production.

Figure 3.1 shows the Sabatier reactor integrated with the Organic Rankine Cycle (ORC) system. This section provides a detailed examination of the Sabatier reactor, including the formulation of the 0-D kinetic equations governing its operation. The system also incorporates a proton exchange membrane (PEM) electrolyzer, which has been specified to operate at a constant capacity of 2 MW. The CO_2 capture subsystem, responsible for supplying the carbon dioxide required for the Sabatier reaction, is presented. Additionally, any CO_2 excess of the Sabatier reactor's consumption is repressurized and injected back into the reservoir to ensure its long-term sustainability, maintain reservoir health, and support renewable operation.

3.3 Modelling of the Geothermal Power Plant

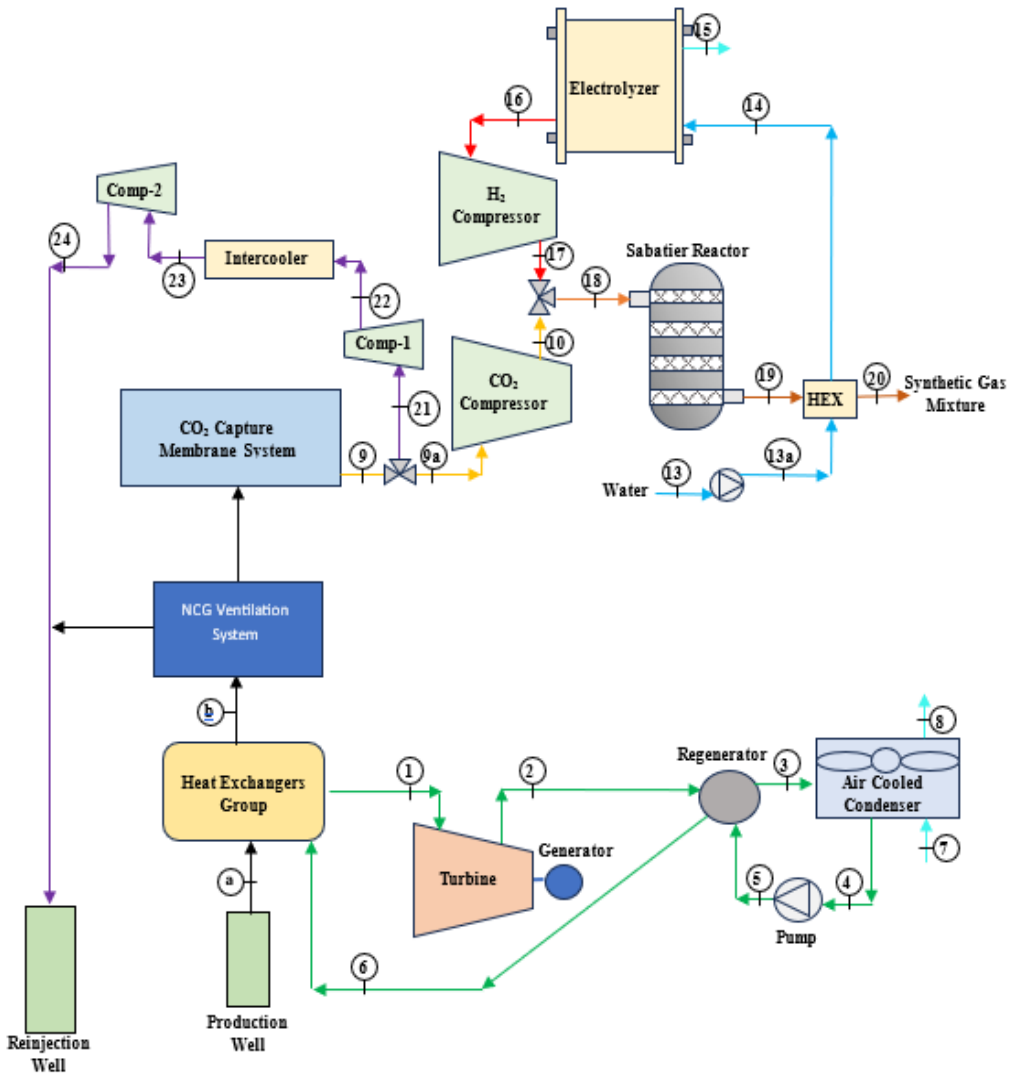

Figure 3.1 Schematic view of the power to synthetic methane production system

In this section, the geothermal system, which is the primary energy source of the system and produces the electrical energy required for hydrogen production, is modeled and detailed using the equations used. In addition, the parameters of the geothermal fluid extracted from the reservoir are provided, and the details of reservoirs in the world and Türkiye are provided.

3.3.1 Selection of the Geothermal Fluid

Reservoir temperature plays a significant role in the installation of geothermal power plants. In locations where the reservoir temperature is 180 °C or higher and where high-enthalpy reservoirs are found, dry or flash type power plants are suitable, while in locations where the reservoir temperature is between 110 and 180 °C, binary systems are used.

In this study, a geothermal reservoir with a temperature of 160 °C was utilized. According to the reservoir classification given in Table 2.4, this reservoir falls into the high enthalpy class. By selecting a reservoir temperature of around 160°C, it became possible to establish a binary-type geothermal system. In Section 2, examples of gases used in binary systems were given, such as R-134a, R141b, n-pentane, and n-butane. In the system created within the scope of this study, R-134a gas was used as the secondary fluid. In addition to the reservoir temperature, other parameters such as reservoir pressure and mass flow rate are provided in Table 3.2.

3.3.2 Heat Exchanger

As mentioned in the previous section, the geothermal system considered within the scope of this study was a binary type. In geothermal plants that use binary systems, the primary fluid refers to the geothermal fluid taken from the reservoir, while the secondary fluid is known as the fluid that is sent to the turbine and used in energy production. In binary systems where the primary fluid, i.e., the geothermal fluid, is not directly sent to the turbine, the heat of the geothermal fluid must be transferred to the secondary fluid sent to the turbine. This task is performed by a heat exchanger installed in the system.

Heat exchangers (HEXs) are used in renewable energy technology systems, temperature-sensitive environments, and systems where energy recovery takes place. (80) HEXs basically consist of fluid inlet and outlet points, sections through which fluids flow, and heat transfer surfaces. As with many components, there are different types of HEXs that serve different purposes. These include plate-type, shell-and-tube-type, regenerative-type, finned-tube-type, coiled-tube-type, double-pipe-type, printed-circuit, and scraped-surface-type HEX, among others. The performance of heat exchangers is influenced not only by their type but also by the thermophysical properties of the fluids, the temperature differences between the fluids, and the materials used.

Table 3.1 Advantages and disadvantages of the heat exchanger types (Bhuvanendran et al., 2023)

HEX Type	Advantages	Disadvantages
Shell and Tube	Flexibility of design, relatively low maintenance cost; suitable for high working temperatures and pressure.	Tube design leads to vibration and stagnation of fluid
Plate	More compact than shell and tube-type HEXs, compact; require lower difference in streams temperature	Relatively challenging to clean, poor pressure resistance and prone to fouling
Coiled tube HEX	Compact design	Difficult to clean and maintain, not suitable for high-viscosity fluids
Double-pipe HEX	Simple construction; suitable for high-viscosity working fluids	Limited heat transfer area

Table 3.1 lists the commonly used types of heat exchangers and their advantages and disadvantages. Shell and tube heat exchangers are widely used due to their ability to operate under high-pressure and temperature conditions and low maintenance costs. In this study, a shell and tube type heat exchanger was used to transfer the heat of the geothermal fluid to the R-134a gas sent to the turbine, thereby generating energy.

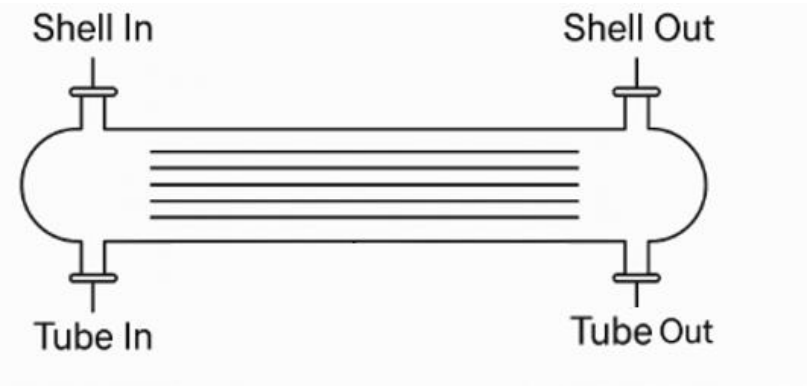

Figure 3.2 Schematic view of the shell and tube type heat exchanger (Kern et al., 1959)

The design parameters of the shell and tube type heat exchanger, which is schematically shown in Figure 3.2 and integrated into the geothermal system within the scope of the study, are shown in Table 3.4. According to this, the HEX in the system is designed to consist of 1 pass and 4000 tubes, each 18 meters long. The heat transfer within the system is calculated using Equation 3.41. Q represents the heat transfer rate, U is the overall heat transfer coefficient, A is the heat transfer area, and ΔT_m is the logarithmic mean temperature difference (LMTD). The LMTD is calculated using Equation 3.2. The heat transfer area A is determined based on the geometry of the heat exchanger as shown in Equation 3.3, where n denotes the number of tubes, D_0 is the outer diameter of each tube, and L is the tube length.

$$Q = U \cdot A \cdot \Delta T_m \tag{3.1}$$

$$\Delta T_m = \frac{(T_{h,in} - T_{c,out}) - (T_{h,out} - T_{c,in})}{\ln\left(\frac{T_{h,in} - T_{c,out}}{T_{h,out} - T_{c,in}}\right)} \tag{3.2}$$

$$A = n \cdot \pi \cdot D_0 \cdot L \tag{3.3}$$

Table 3.2 Modelling parameters of integrated system

Parameters of Heat Exchanger			
Heat Exchanger	Shell and Tube	Overall Heat Transfer Coefficient	$1\ kW/m^2K$
Type	Counterflow	L_{hx} (Tube length per pass)	18 meter
Number of Pass	1	D_i (Inner diameter of the tube)	$16x10^{-3}$meter
Number of Tubes	4000	R_{wall} (Wall thickness)	$3x10^{-3}$ meter
D_o (Outer diameter of the tube)	$22x10^{-3}$ meter	K_{tube} (Thermal conductivity of tube)	$63\ W/mK$
Parameters of Air-Cooled Condenser		**Parameters of Sabatier Reactor**	
$T_{ambient}$	291 K	Catalyst Type	(Ni/ZrO_2)
W_{fan}	600 kW	Operating Temperature	200 °C
$\dot{m}_{air}$	3240 kg/s	Operating Pressure	635 kPa
P_{air}	101,325 kPa	Type	Tubular Fixed Bed
Parameters of Geothermal Fluid			
Inlet Pressure of Geothermal Fluid	780 kPa	Inlet Temperature of Geothermal Fluid	160.45 °C
Mass Flow Rate of Geothermal Fluid		120.7 kg/s	

3.3.3 Turbine and Generator

Turbines in geothermal systems are referred to as the heart of organic Rankine cycles because turbines produce mechanical work by expanding high-temperature and high-pressure organic fluid before it changes from the vapor phase to the liquid phase,

and electricity is generated by the rotation of the generator shaft (EMS, 2025). In this study, high-pressure and high-temperature R-134a gas was sent to the turbine, and the generator produced the electrical energy needed by all other systems through the mechanical work generated by the expansion of the R-134a gas in the turbine.

Under ideal conditions, the enthalpy at the turbine outlet (h_{2s}) is calculated using the inlet entropy and inlet pressure. However, due to irreversibility in real turbines, which are not ideal, the calculation is performed using the isentropic efficiencies of the turbines. In this study, the isentropic efficiency of the turbine (ηst) is assumed to be 0.8.

$$\eta_{st} = (h_1 - h_2)/(h_1 - h_{2s}) \tag{3.4}$$

The enthalpy at the turbine outlet is calculated using Equation 3.4, and the isentropic efficiency is used to determine the power generated. The efficiency of the generator used in the system is also essential at this point, and the efficiency of the generator used in this study has been determined to be 98%. The power generated is found by taking the difference between the enthalpies at the turbine inlet and outlet and multiplying it by the flow rate of the organic fluid passing through the turbine and the generator efficiency. Equation 3.5 shows the method of calculating the power obtained.

$$\dot{W}_{turbine} = \dot{m}_{R_{134a}} \cdot (h_1 - h_2) \cdot \eta_{Gen} \tag{3.5}$$

3.3.4 Air Cooled Condenser and Pump

The organic fluid used in the Organic Rankine Cycle must be cooled after exiting the turbine in order to be reused efficiently. At this point, air- or liquid-cooled condensers are used. This study used an air-cooled cooling system, in which heat transfer occurs from the organic fluid to the ambient air. Since air cooling systems do not require a water source, they can be used in arid regions and are more sustainable. (Takano et al., 2016) In this study, the organic fluid exiting the turbine, which is still at a high temperature, is sent to the air-cooled condenser, where its temperature is

reduced, enabling the organic fluid to be reintroduced into the cycle. The design parameters of the cooling system used in this study are provided in Table 3.2.

The temperature and pressure of the organic fluid coming out of the air-cooled condenser decrease, and a pump is used in the system to complete the cycle of the organic fluid. To determine the power drawn by the pump, the enthalpies at the pump inlet and outlet must be known.

Here, it is assumed that the organic fluid exiting the air-cooled condenser is saturated and completely liquid. Like the turbine, the pump also has an isentropic efficiency, which is assumed to be 0.8 in this study. Thus, the power drawn by the pump can be calculated using Equations 3.6 and 3.7. Here, v_4 is the specific volume of the fluid. The power consumed by the pump is calculated using Equation 3.8.

$$h_{5s} = h_4 + v_4 \cdot (P_5 - P_4) \quad 3.6$$

$$h_5 = (h_{5s} - h_4)/(\eta_{s\,pump}) + h_4 \quad 3.7$$

$$\dot{W}_{pump} = \dot{m}_{R_{134a}} \cdot (h_5 - h_4) \quad 3.8$$

3.4 Modelling of the Proton Exchange Membrane Electrolyser

A Sabatier reactor was used to produce synthetic methane, which was the main objective of this study. The Sabatier reaction requires hydrogen gas by its very nature. A PEM Electrolyser was used to produce the hydrogen needed by the system. The power required for the electrolyser to operate is obtained from a geothermal system, thereby creating a system that operates entirely on renewable energy.

Some assumptions have been made in the electrolyser used in this study, as follows:

- The PEM electrolyser used operates at 100% capacity.
- The electrolyzer is assumed to operate at steady-state with a constant power input of 2 MW throughout the analysis..
- It was assumed that the gases behave as ideal.
- Changes in kinetic and potential energy are neglected.
- The operating temperature of the electrolyser is 60°C

- The amount of hydrogen produced per unit of energy is calculated using an experimentally determined correlation.

The hydrogen produced in the PEM electrolyser used is calculated using Equation 3.9. According to the assumptions made in this study, the amount of hydrogen produced is calculated by multiplying the power of the electrolyser by the energy used per unit. Additionally, since the produced hydrogen gas is used for synthetic methane production in the Sabatier reactor, it must be pressurized to the appropriate pressure. For this purpose, a compressor is used, and the energy consumed by this compressor is calculated using Equation 3.10. The amount of H_2 produced per unit of energy, derived from experimental studies reported in the literature, is shown in Equation 3.11 (Atak et al., 2024).

$$\dot{m}_{h_2} = \in \cdot \ W_{electrolyzer} \tag{3.9}$$

$$\dot{W}_{H_2\ compressor} = \ \dot{m}_{16} \cdot (h_{17} - h_{16}) \tag{3.10}$$

$$\in = \ -0.236 \cdot EL^5 + 1.278 \cdot EL^4 - 2.539 \cdot EL^3 + 2.337 \cdot EL^2 + 0.1991 \tag{3.11}$$

3.5 Modelling of the Carbon Dioxide Capture System

Geothermal fluids extracted from sources used in geothermal energy systems contain non-condensable gases. As detailed in the previous section, with the increasing climate change and acceleration of global warming, it is very important for sustainability to send NCGs back to the reinjection well instead of releasing them into the atmosphere. In order to send these gases back to the reinjection well, they must first be separated from the geothermal fluid.

The configuration designed to capture non-condensable gases (NCGs) is illustrated in Figure 3.1. In this system, the geothermal fluid exiting the heat exchanger is reinjected into the earth's crust through a reinjection well to maintain reservoir continuity and preserve the renewable characteristics of the energy produced. Although the reinjected geothermal fluid contains NCGs, these gases remain in the vapor phase due to their inability to condense under reservoir conditions.

In this study, certain assumptions were made in order to obtain the necessary CO_2 gas. Thus, with these assumptions, carbon dioxide required for synthetic methane production in the Sabatier reactor is produced. These assumptions are as follows:

- The geothermal fluid coming out of the heat exchanger is completely in liquid phase.
- It is assumed that 100% of the non-condensable gas is CO_2.

The CO_2 produced must be brought to a suitable pressure for the Sabatier reaction to take place. A compressor has been integrated into the system to bring the CO_2 to the appropriate pressure. The power consumed by this compressor is calculated using Equation 3.12.

$$\dot{W}_{CO_2 COMPRESSOR} = \dot{m}_9 \cdot (h_{10} - h_9) \quad 3.12$$

If the amount of carbon dioxide gas used with hydrogen in the Sabatier reactor exceeds the amount required in the Sabatier reactor, the excess portion is returned to the reservoir through a two-stage pressurization and intercooler system. This ensures the continuity of the reservoir and supports production for many years. The isentropic efficiencies of the compressors used here are determined to be 0.85. The following equations were used to calculate the power consumption of the two compressors.

$$h_{22} = (h_{22s} - h_{21})/(\eta_{s_{pump}}) + h_{21} \quad 3.13$$

$$h_{24} = (h_{24s} - h_{23})/(\eta_{s_{pump}}) + h_{23} \quad 3.14$$

$$\dot{W}_{CO_2 COMP-1} = \dot{m}_{CO_2} \cdot (h_{21} - h_{22}) \quad 3.15$$

3.6 Modelling of the Sabatier Reactor

Sabatier reactors represent a critical technology for mitigating carbon accumulation, which has become an increasingly pressing global issue. The rising concentration of carbon dioxide in the atmosphere contributes significantly to the acceleration of global warming. To address this challenge, instead of releasing CO_2 into the atmosphere, it can be captured and utilized. This approach not only reduces environmental carbon accumulation but also enables its conversion into fuel through

appropriate technological systems. The primary application areas of Sabatier reactors are outlined as follows.

In Section 2, Equations 2.2, 2.3, and 2.4 were used to illustrate the working mechanism of the Sabatier reaction. However, as mentioned in the previous section, the reverse water-gas shift reaction (RWGS) and carbon monoxide methanation, expressed by Equations 2.3 and 2.4, are dominant at temperatures of 600 °C and above, while at temperatures below this, only the reaction described by Equation 2.2 can occur. In this study, since the operating temperature of the Sabatier reaction was selected as 200°C, RWGS and CO methanation were not included in the calculations. A nickel-based zirconia-supported catalyst (Ni/ZrO_2) was used to increase reaction efficiency and prevent carbon buildup within the reactor. The parameters used in modeling the Sabatier reactor are provided in Table 3.2.

Takano et al. described the reaction kinetics for the Sabatier reaction as follows (Takano et al., 2016). Where, p_{CO_2}, p_{H_2}, p_{CH_4}, and p_{H_2O} represent the partial pressures of carbon dioxide, hydrogen, methane, and water, respectively. The forward and backward reaction constants are denoted as k_f and k_r, respectively. The constants K_{CO_2}. and K_{H_2O} in the equation represent the adsorption equilibrium constants. R denotes the universal gas constant, E_a and ΔH represent the activation energy and enthalpy change of adsorption, respectively.

$$r_{CH_4} = k_f \frac{K_{CO_2} \cdot p_{CO_2} \cdot p_{H_2}^{0.5}}{(1+K_{CO_2} \cdot p_{CO_2})} - k_r \frac{K_{H_2O} \cdot p_{CH_4}^2 \cdot p_{H_2O}}{(1+K_{H_2O} \cdot p_{H_2O})^2} \quad 3.16$$

$$k_j = k_{j,0} \cdot e^{(-\frac{E_a j}{RT})} \quad 3.17$$

$$K_i = K_{i,0} \cdot e^{(-\frac{\Delta H_i}{RT})} \quad 3.18$$

The values for kinetic parameters are given in the study by Choi et al. (2021) and discussed in detail. After calculating the reaction rate as the production/destruction rate of species, the mass balance is applied to the control volume for each species.

$$CO_2 \ : \ \dot{m}_{CO_{2,in}} - MW_{CO_2} \cdot r = \ \dot{m}_{CO_{2,out}} \quad 3.19$$

$$H_2 \ : \ \dot{m}_{H_{2,in}} - 4MW_{H_2} \cdot r = \ \dot{m}_{H_{2,out}} \quad 3.20$$

$$CH_4 \ : \ \dot{m}_{CH_{4,in}} + MW_{CH_4} \cdot r = \ \dot{m}_{CH_{4\,out}} \quad 3.21$$

$$H_2O \ : \ \dot{m}_{H_2O_{,in}} + 2MW_{H_2O} \cdot r = \ \dot{m}_{H_2O,out} \quad 3.22$$

3.7 Calculation of the Thermal Efficiency of the System

In this study, the thermal efficiency of the system was calculated as the ratio of the net electrical work output of the system to the heat input from the geothermal system. The geothermal system is an ORC-type system, as described in detail in this section, and provides energy to all other components used in synthetic methane production, with the energy produced denoted as $\dot{Q}_{in,geo}$ .The network output consists of the pump and fan used in the ORC system, the CO_2 and H_2 compressors that bring the hydrogen and carbon dioxide required for the Sabatier reaction to the appropriate pressure, the compressors that send CO_2 to the reservoir when necessary, and the PEM electrolyser responsible for hydrogen production. Equation 3.23 shows the calculation method for the network obtained from the system created within the scope of the study. The energy obtained from the geothermal system is shown in Equation 3.24.

$$\dot{W}_{net} = \dot{W}_{turbine} - \dot{W}_{fan} - \dot{W}_{CO_2,comp} - \dot{W}_{H_2,comp} - \dot{W}_{PEME} - \dot{W}_{CO_2,recomp} \quad 3.23$$

$$\dot{Q}_{in,geo} = \dot{m}_{geo} \cdot (h_a - h_b) \quad 3.24$$

In Organic Rankine Cycles (ORCs), the thermal system efficiency is typically determined by the ratio of the net work output ($\dot{W}_{net}$) to the geothermal heat input ($\dot{Q}_{in,geo}$). However, in the system the production of methane via the Sabatier reactor introduces an additional form of chemical energy which must be incorporated into the efficiency calculation. Consequently, the system not only generates mechanical or electrical work but also yields a chemical energy output in the form of synthetic CH_4 fuel. This chemical energy contribution is therefore essential for an accurate assessment of the system's total efficiency.The method used to calculate the system's total efficiency is shown in Equation 3.25. Here, $\dot{m}_{syngas}$ represents the flow rate of the synthetic fuel produced, while LHV_{syngas} denotes the Lower Heating Value (LHV)

of the synthetic fuel produced. LHVis equal to the higher heating value minus the latent heat of the condensed water vapor. LHV is determined based on the assumption that the water produced during combustion remains in the vapor phase, and it is therefore typically regarded as a constant under standard conditions. The LHV_{syngas} used in Equation 3.25 is determined by multiplying the lower heating value of each gas in the mixture by its molar fraction and then summing these values.

$$\eta_{th} = \frac{\dot{W}_{net} + (LHV_{syngas} \cdot \dot{m}_{syngas})}{\dot{Q}_{in,geo}} \quad 3.25$$

In this section, the reaction kinetics and mechanisms of all components used in sequence are presented and detailed. The modeling equations provided were transferred to the EES program and solved. The results obtained are detailed in the next section.

3.7 Exergy Analysis of the System

In evaluating the performance of engineering systems, solely examining and calculating the energy balance is often insufficient, as the quality of energy changes in addition to its quantity. Exergy analysis addresses this limitation by assessing the potential of system components to perform work, identifying sources of losses, and revealing irreversibilities within the system (Dincer et al., 2012). It plays a crucial role in pinpointing where inefficiencies arise and serves as a guide for system optimization. Moreover, since exergy efficiency provides a more realistic measure of system performance compared to conventional energy efficiency, it is widely employed to assess both the sustainability and environmental impact of engineered systems (Rosen et al., 2001). Therefore, exergy analysis constitutes a key metric not only for engineering efficiency but also for economic and ecological evaluations (Karellas et al., 2016). In the present study, both physical and chemical exergy were calculated. Since synthetic methane is produced through the Sabatier reaction, both chemical exergy and physical exergy must be considered. Equation 3.26 presents the method for estimating total exergy, where $\overline{ex}_i^{PH}$ denotes the physical exergy and $\overline{ex}_i^{CH}$ represents the chemical exergy.

$$\overline{ex}_i = \overline{ex}_i^{PH} + \overline{ex}_i^{CH} \quad 3.26$$

3.7.1 Physical Exergy

Physical exergy is related to the temperature and pressure of the components and types in the system. The physical exergy calculation is performed using Equation 3.27. Here, $\bar{s}$ and $\bar{h}$ are the specific entropy and enthalpy, respectively, and T0 indicates the reference temperature. The entropy and enthalpy values indicated by the subscript 0 are the values at the reference temperature (298) and reference pressure (100 kPa). The specific enthalpy and entropy of the gases used in the study at the reference temperature and pressure are given in Table 3.3.

$$\overline{ex}_i^{PH} = \bar{h}_i - \overline{h_0} - T_0 \cdot (\bar{s}_i - \bar{s}_0) \qquad 3.27$$

Table 3.3 Reference specific enthalpy and entropy values at the 298.15 K and 101.325 kPa (Moran et al., 2010)

Species	**Specific Enthalpy, $\overline{h_0}$, (kJ/kmol)**	**Specific Entropy, $\overline{s_0}$, (J/kmol-K)**
H_2O	-241.811	188.7
CO_2	-393.486	213.7
O_2	0	205.03
H_2	0	130.6
R134a(Gas)	25.22	93.88
Air	298.15	192
CH_4	-74.87	188.26

3.7.2 Chemical Exergy

Chemical exergy is taken into account at points where combustion, fuel cell systems, and energy conversion systems are present in a system. Within the scope of this study, chemical exergy calculations should also be performed for the electrolyser that enables hydrogen production and the Sabatier reactor where synthetic methane

production occurs. Chemical exergy is related to the chemical composition of a system. The method for calculating chemical exergy is shown in Equation 3.28.

$$\overline{ex}_j^{CH} = \sum X_j \cdot \overline{ex_j}^{ch} + \bar{R} \cdot T_0 \cdot \sum X_j \cdot \ln(X_j) \quad 3.28$$

Where, X_j represents the mole fractions of the species present in the system, while $\overline{ex_j}^{ch}$ represents the chemical exergy.

Table 3.4 Chemical exergy values of species at 298.15 K and 101.325 kPa (Moran et al., 2010)

Species	**Standard Chemical Exergy, $\overline{ex}_j^{CH}$, (kJ/kmol)**
H_2O	8.635
CO_2	14.175
H_2	235.250
O_2	3.950
CH_4	824.350

3.7.3 Exergy Balance

Control volumes are generally used to calculate exergy balance. Separate control volumes are created for all components used in the system, physical and chemical exergy calculations are performed, and the exergy balance shown in Equation 3.29 is used for each component to determine exergy destruction.

$$0 = \sum_j \dot{E}_{Q,j} - \dot{E}x_{W_{cv}} + \sum_i \dot{E}x_i - \sum_j \dot{E}x_j - \dot{E}_{xD} \quad 3.29$$

$\dot{E}x_i$ and $\dot{E}x_j$ are used to calculate the exergy of the types entering and leaving the control volume. $\dot{E}_{Q,j}$ denotes the exergy transferred by heat, while $\dot{E}_{xD}$ is defined as the exergy destruction rate of the system components in the control volume. $\dot{E}x_{W_{cv}}$ indicates the total exergy transferred due to work. Equations 3.30-3.32 provide the

equations used to calculate the exergy change in the control volume. Table 3.5 shows the exergy balance equations for all control volumes.

$$\dot{E}x_i = \dot{m}_i \cdot \overline{ex}_i \quad 3.30$$

$$\dot{E}x_e = \dot{m}_e \cdot \overline{ex}_e \quad 3.31$$

$$\dot{E}_{Q,j} = \dot{Q}_j \cdot (1 - \frac{T_0}{T_j}) \quad 3.32$$

3.7.4 Exergetic Performance Assessment

Exergy efficiency enables a better thermodynamic performance evaluation of the system (Kazim, 2004). The exergy efficiency of the system $\varepsilon_{\text{system}}$ is defined by considering both the mechanical work output and the chemical exergy of the produced methane. Specifically, it is calculated as the ratio of the sum of the net work output ($\dot{W}_{net}$) and the chemical exergy of methane ($\dot{E}x_{CH4}$) to the exergy input provided by the geothermal fluid ($\dot{E}x_{geo\ fluid}$). Calculating the exergy efficiency of a system allows for a much better evaluation of its thermodynamic performance. (Kazim, 2004).. Equation 3.33 also shows the exergy calculation of the methane gas produced.

$$\varepsilon_{\text{system}} = \frac{\dot{W}_{net} + \dot{E}x_{CH4}}{\Delta\dot{E}x_{geo\ fluid}} \quad 3.33$$

$$\dot{E}x_{CH4} = \overline{ex}_{CH_4} \cdot \dot{m}_{CH_4,out} \quad 3.34$$

$$\Delta\dot{E}x_{geo\ fluid} = \dot{m}_{geo} \cdot ((h_a - h_b) - T_0 \cdot (s_a - s_b)) \quad 3.35$$

Table 3.5 Control volume and exergy balance equations of all components

Components	**Control Volume**	**Exergy Balance**
HEX-1	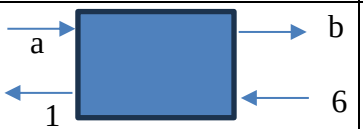	$\dot{E}x_a - \dot{E}x_b + \dot{E}x_6 - \dot{E}x_1 - \dot{E}x_{D,HEX1}=0$
Turbine		$\dot{E}x_1 - \dot{E}x_2 - \dot{E}x_{turbine} - \dot{E}x_{D,turbine}=0$
ACC		$\dot{E}x_3 - \dot{E}x_4 + \dot{E}x_7 - \dot{E}x_8 - \dot{E}x_{D,ACC}=0$
Pump		$\dot{E}x_4 - \dot{E}x_5 + \dot{W}_{pump} - \dot{E}x_{D,Pump}=0$
CO_2 Compressor-1		$\dot{E}x_9 - \dot{E}x_{10} + \dot{W}_{comp_1} - \dot{E}x_{D,comp,1}=0$
CO_2 Compressor-2	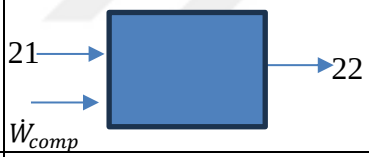	$\dot{E}x_{21} - \dot{E}x_{22} + \dot{W}_{comp_2} - \dot{E}x_{D,comp,2}=0$
CO_2 Compressor-3		$\dot{E}x_{23} - \dot{E}x_{24} + \dot{W}_{comp_3} - \dot{E}x_{D,comp,3}=0$
H_2 Compressor		$\dot{E}x_{16} - \dot{E}x_{17} + \dot{W}_{comp_{H_2}} - \dot{E}x_{D,comp,H_2}=0$
Electrolyser		$\dot{E}x_{14} - \dot{E}x_{16} + \dot{W}_{Elec} - \dot{E}x_{15} - \dot{E}x_{D,Elec}=0$
Sabatier Reactor		$\dot{E}x_{18} - \dot{E}x_{19} - \dot{E}x_{D,Sabatier}=0$
HEX-2	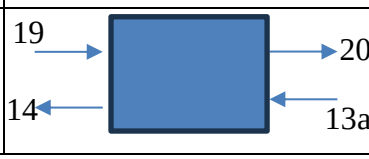	$\dot{E}x_{19} - \dot{E}x_{20} + \dot{E}x_{13a} - \dot{E}x_{14} - \dot{E}x_{D,HEX2}=0$

CHAPTER FOUR
TECHNO-ECONOMIC ANALYSIS OF THE SYSTEM

4.1 Introduction

In this chapter, geothermal power plants, which provide a continuous heat source throughout the day, are one of the most sustainable renewable energy sources with the potential to integrate with power-to-fuel technologies. By operating electrolysers and carbon dioxide systems powered by geothermal energy, methane gas is produced through the Sabatier reaction, creating a portable form of energy. In such systems, evaluating the geothermal plant together with the methanation unit is critical in terms of scalability, efficiency, and capital and operating costs. In power-to-methane systems, system efficiency, investment costs, and interest rates are very important factors in the economic analysis of the system. Studies conducted in recent years have shown that production costs are in the range of 0.24–0.30 €/kWh (Götz et al., 2016). In optimized systems, production levels of 3.51–3.88 €/kg have been demonstrated Morgenthaler et al., 2020).

Techno economic analysis (TEA) is one of the most important methods used to evaluate the feasibility and sustainability of energy production systems. TEA is an integrated assessment methodology that combines engineering-based technical performance modeling with economic evaluation to determine the feasibility and competitiveness of a process or technology. In essence, TEA links mass and energy balances, process design, and system efficiency with capital expenditures (CAPEX) and operational expenditures (OPEX) to estimate key economic indicators such as the minimum product selling price, levelized cost, net present value (NPV), and internal rate of return (IRR). This approach is widely applied to guide investment decisions, prioritize research and development, and evaluate the commercial potential of emerging technologies (Chai et al., 2022). Subsequently, the economic dimension of the desired system is calculated using capital expenditure (CAPEX) and operational expenditure (OPEX) estimates (Energy, U. (2004). Life Cycle Cost Assessment (LCCA) is extremely important in engineering systems and forms the basis of energy economics calculations. The calculation of LCCA may include the project's investment costs, labor, and maintenance costs necessary for the system to operate smoothly

throughout its lifetime, which can only be done by calculating CAPEX and OPEX costs and adding the change in the value of money over time to the total cost. Each system also possesses a residual value at the end of its operational life, referred to as the scrap value, which must be incorporated into LCCA calculations. TEA integrates the engineering aspects of system design with financial assessments, thereby enabling a comprehensive evaluation of the technical and economic sustainability of a given process (U.S. Department of Energy, 2004). The cash flow of an engineering system throughout its economic lifetime can be represented by a cash flow diagram, as illustrated in Figure 4.1. In this representation, the horizontal axis denotes time, while the vertical arrows indicate cash flows, with negative arrows corresponding to expenditures and positive arrows representing revenues.

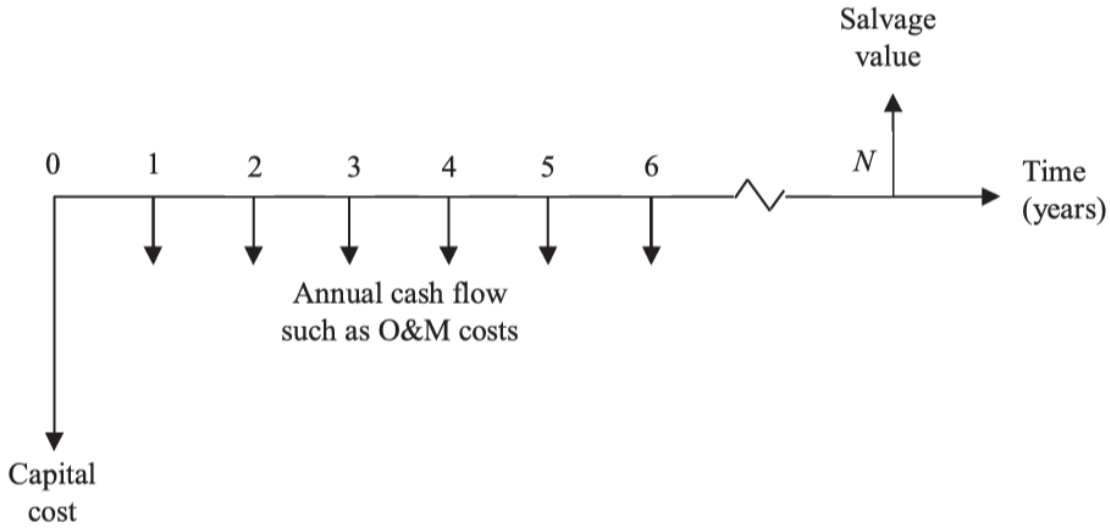

Figure 4.1 Cash flow diagram during the lifetime (Dhillon et al., 2009)

In the TEA of a facility that utilizes geothermal resources for renewable energy production and synthetic methane generation, the largest expenditure corresponds to detailed installation costs, followed by operating expenditures (OPEX). On the revenue side, electricity and methane sales constitute the primary sources of income for the system. Some of the fundamental equations employed in the life-cycle cost analysis (LCCA) process are presented below (Dhillon et al., 2009).

$$P = \frac{F}{(1+i)^N} \quad (4.1)$$

$$U = P\left(\frac{i}{1-(1+i)^{-N}}\right) \quad (4.2)$$

$$F = U\left(\frac{(1+i)^N-1}{i}\right) \quad (4.3)$$

P represents the present value of money, F represents the future value of money, U represents the uniform series amount, i represents the interest rate (%), and N represents the economic life (years).

In the previous section, the system integrated into the geothermal power plant and producing synthetic methane was introduced and detailed using thermodynamic calculation equations. Accordingly, the hydrogen required for methane production is obtained from the PEM electrolyser, while carbon dioxide is extracted from the non-condensable gas present in the geothermal fluid. The energy requirements of all components used in the study are produced by an ORC-type geothermal power plant, thus creating a completely renewable, off-grid system unaffected by environmental and seasonal conditions, sustainable, and highly continuous. Table 4.1 lists the components used in the system established for synthetic methane production and the design parameters of these components. Certain assumptions have been made for the techno-economic analysis of the system developed within the scope of this study. Accordingly, the system life has been set at 30 years, the operating capacity of the system, which is common in geothermal energy systems, has been determined as 95%, and the annual operating time has been set at 8322 hours. The annual interest rate has been set at a fixed rate of 10%. The salvage value ratio (SV) of the developed system has also been set at 20%.

4.3 CAPEX (Capital Expenditure) Costs

The largest expense of the system created within the scope of the study is the investment cost. In other words, CAPEX refers to the initial investment cost for setting up a system, including the construction, commissioning processes, and equipment expenses of a one-time project. Sub-items include drilling costs, reservoir preparation for production, piping, land costs, all construction costs, engineering and project costs,

and grid connection costs. Unexpected expenses are also included, which are generally around 10%. Chapter 3 provided detailed information on the scope of the study and the design and operating parameters of the components used. Table 4.1 lists all costs used in the CAPEX cost calculation. The correlations obtained from the literature were used to calculate the component costs, as shown in Table 4.1.

The cost calculation methods for the components used in the system designed within the scope of this study are presented in the table below. The equations employed, however, are derived from studies conducted in different years, and the calculated costs are valid for those specific years. Updating these costs to present-day values is crucial for ensuring the accuracy and relevance of the study. The costs of the components used in the system are calculated using the given functions for their reference year and subsequently normalized using the cost index (CEPCI). CEPCI is a cost index widely used in the engineering industry to track annual changes in plant and equipment costs and to update historical cost data to current-year values. CEPCI comprises four main subcomponents—equipment, buildings, construction labor, and engineering & supervision—whose cost variations collectively determine the overall index value. This index provides a standardized method for adjusting past cost data and facilitates the comparison of investments across different years. Equation 4.4 shows the process of normalizing the cost of a system component using the CEPCI index (Atak et al., 2025).

$$Z_k = Z_{ref} \cdot \left(\frac{CEPCI_{2025}}{CEPCI_{ref}}\right) \quad 4.4$$

Table 4.1 Correlations of the cost for the components

Component	Equations	References
Heat Exchanger	$C=k \cdot A^n$	(Kumana et al., 1984)
Turbine+Generator	$C=1.23 \cdot E6(n_{stages}/2)^{0,5} \cdot (SP/0,18)^{1,1}$	(Jalili et al., 2023)
Regenerator	$C=k \cdot A^n$	(Kumana et al., 1984)
ACC	$C=L/(Z)(X)-586+(39,2) \cdot (R)$	(Yilmaz et al., 2020)
Pump	$200 \cdot Power(kW)^{0,66}$	(Jalili et al., 2023)
CO_2 Compressor	$33032 \cdot (Power(kW)/445)^{0.67}$	(Jalili et al., 2023)
H_2 Compressor	$33032 \cdot (Power(kW)/445)^{0.67}$	(Jalili et al., 2023)
PEM	1500*kW	RPOW. (2025, May 22)
Heat Exchanger	$C=k \cdot A^n$	(Kumana et al., 1984)
Sabatier Reactor	$2.86 \cdot 106(Volume(m^3)/0.71)^{0.6}$	(Jalili et al., 2023)
CO_2 Capture System	-	(Yılmaz et al., 2020)
Contingencies	-	
Construction &	-	(NS Energy., 2019)
$CEPCI_{1984}$	322.7	(Chemical Engineering, 2025)
$CEPCI_{2019}$	607.5	(Chemical Engineering, 2025)
$CEPCI_{2020}$	596.2	(Chemical Engineering, 2025)

Table 4.1 Continued		
$CEPCI_{2022}$	816	(Chemical Engineering, 2025)
$CEPCI_{2023}$	797.9	(Chemical Engineering, 2025)
$CEPCI_{2025}$	800.2	(Chemical Engineering, 2025)

4.3 OPEX (Operational Expenditure) Costs

OPEX costs are all the expenses incurred to ensure the healthy continuation of a business or facility's daily operations. These include maintenance, production, sales, marketing, general facility expenses, personnel expenses, electricity, water, office expenses, and all other items that fall under the OPEX category. These expenses listed under OPEX are ongoing expenditures used to ensure the continuity, sustainability, and efficiency of a business and are also of great importance in terms of financial management. Since geothermal fluids can be acidic and have the potential to corrode equipment, operating and maintenance costs vary depending on the chemical composition of the steam and brine at each facility. According to the collected data, the average annual operating and maintenance cost is approximately $129/kW, ranging from $75 to $224/kW. Since the system considered in the scope of the study generates 6.5 MW of power, annual OPEX expenses can be calculated at around $880,000.

4.4 Calculation of Levelized Costs

This calculation normalizes costs over time by factoring in investment costs (CAPEX), operating expenses (OPEX), and the present value of the output produced over the system's lifetime. The Levelized Cost calculation covers not only a single point in time but all costs from the project's construction onwards, thereby eliminating the need for instantaneous or variable cost estimates and establishing a more reliable basis for system investment. Since synthetic methane production is carried out within the scope of this study, the following equations are used in the Levelized Cost of

Methane (LCOM) calculation. Here, n shows the lifetime of the facility (20 years), while the discount rate (%10) reflects the time value of money and is used to calculate the present net value of future costs and revenues. A report published in 2023 indicated methane sales prices ranging from $1.5/kg to $3.5/kg and calculated with the Equations 4.5-4.7 (Al-Breiki et al., 2023). Due to rising prices in recent years as a result of geopolitical tensions, the methane sales price was set at $3 per kg for this study.

$$Total\ Lifetime\ Cost = \sum_n \frac{Total\ CAPEX\ and\ OPEX_n}{(1+discount\ rate)^n} \quad 4.5$$

$$Total\ Lifetime\ Output = \sum_n \frac{Methane\ Production_n}{(1+discount\ rate)^n} \quad 4.6$$

$$Levelized\ Cost\ of\ Methane = \sum_n \frac{Total\ Lifetime\ Cost}{Total\ Lifetime\ Output} \quad 4.7$$

The system developed within the scope of this study can also calculate the payback period for methane sales. To perform this calculation, the annual methane production, methane sales price, and total investment costs must be known. The following equations can be used to calculate the system's payback period. Here, LAC (Levelized Annual Cost)is a cost due to the market cost of methane production in $/year, $C_{L_{CH4}}$ unit cost of methane produced and $\dot{m}_{L_{CH4,yearly}}$ shows total methane produced annually. (Dhillon., 2009). Equation 4.9 shows the method for calculating the payback period of the total investment. Here, TCI (Total Cost of Investment) is indicated and represents the total investment cost, Simple Payback Period (SPP) indicates the number of years required for an investment to recover its initial cost through annual net revenues or savings

$$C_{L_{CH4}} = \frac{LAC}{\dot{m}_{L_{CH4,yearly}}} \quad 4.8$$

$$SPP = \frac{TCI}{LAC}\left(\frac{\$}{\frac{\$}{year}} = year\right) \quad 4.9$$

CHAPTER FIVE
RESULTS AND DISSCUSSION

5.1 Introduction

This section includes the results of a system that produces hydrogen and carbon dioxide using an electrolyser and carbon dioxide utilization system integrated with the Organic Rankine Cycle discussed in Section 3, and a system that produces synthetic methane gas using a Sabatier reactor. The operating parameters of ORC, geothermal source, and Sabatier reactor are given in Section 3. In addition, the modeling equations of the ORC, ACC, geothermal system pump, CO_2 and H_2 compressors, and Sabatier reactor are given in the previous section. The modelling equations given in Section 3 are entered and solved, and the parametric studies are conducted using EES. The modeling equations given in Section 3 were entered into the EES program and solved; parametric studies were conducted using EES.

The parametric analysis performed using the EES program obtained results by changing the organic fluid used in the ORC system. Here, the effect of using different gases such as R134a, R124a, R142b, isobutane, R227ea, and R290 in the ORC system on the total system efficiency was investigated. Additionally, the total thermal efficiency of the system was calculated based on the different working fluids used in the ORC system. In another parametric analysis conducted as part of the study, the percentage ratios of the gases formed as a result of the Sabatier reaction were also calculated.

5.2 Effect of the Working Fluid of the ORC

The operating parameters for all components in the system established for synthetic methane production in the previous section are provided. Table 4.1 provides the parameters used in the study to demonstrate the effect of different organic fluids on the thermal efficiency of the system and the net power produced.

Figure 5.1 shows how the system efficiency changes according to various working fluids. As shown in Figure 5.1, the use of different organic fluids has caused significant changes in the system's thermal efficiency due to differences in their thermodynamic properties. The lowest efficiency was obtained when isobutane was used in the ORC system. However, the results illustrate that when R290 is used as the ORC working fluid, it achieves the highest thermal efficiency among the other working fluids that were examined.

In another parametric study conducted in EES as part of this work, the effect of the working fluid on the net power produced in the system was also calculated. Figure 5.1 shows the effect of different working fluids on the net power produced. According to this, the lowest net power output was observed when isobutane was used in the ORC system, while R290 achieved the highest net 4353 kW power output and %20 efficiency among the other working fluids examined when used as the ORC working fluid.

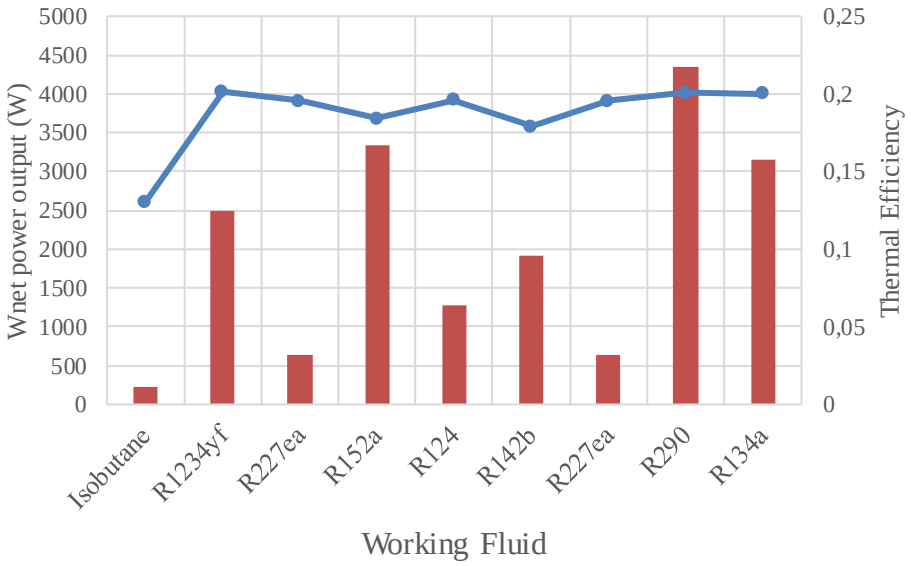

Figure 5.1 Effect of different ORC working fluids on the energy efficiency and net power output of the integrated system

5.3 Effect of Reaction Temperature on the Reaction

Temperatures that are not very high thermodynamically increase the methane formation yield in the Sabatier reaction, and it has been observed in literature studies that they promote the reaction equilibrium in the direction of methane formation. Within the scope of this study, the necessary analyses were performed assuming that the Sabatier reaction occurs at 200 °C. However, the effect of the Sabatier reaction temperature on the reaction and its effects on the molar fractions of the species formed as a result of the reaction were also investigated. In this parametric analysis performed in the EES program, the following values were accepted as initial conditions. To investigate the effect of reaction temperature, the reactor temperature was increased from 200 °C to 600 °C, and the effect of temperature increase on species such as CO_2, H_2, CH_4, and H_2O was examined.

Thermodynamically moderate temperatures increase methane formation efficiency in the Sabatier reaction, and literature studies have observed that these temperatures promote reaction equilibrium toward methane formation. Within the scope of this study, the necessary analyses were performed assuming that the Sabatier reaction occurs at 200 °C. However, the effect of the Sabatier reaction temperature on the reaction and its effects on the molar fractions of the species formed as a result of the reaction were also investigated. In this parametric analysis performed in the EES program, the following values were accepted as initial conditions. To investigate the effect of reaction temperature, the reactor temperature was increased from 200 °C to 600 °C, and the effect of the temperature increase on species such as CO_2, H_2, CH_4, and H_2O was examined.

Figure 5.2 shows the change in hydrogen gas obtained from an electrolyser operating entirely on renewable energy from a geothermal power plant, depending on different reactor temperatures. When the reactor temperature is at its initial condition of 200°C, hydrogen is found at the lowest rate at the end of the reaction, and an increase in this rate is observed with an increase in reactor temperature. The high proportion of hydrogen in the gas mixture formed at the end of the reaction negatively affects the total efficiency of the system.

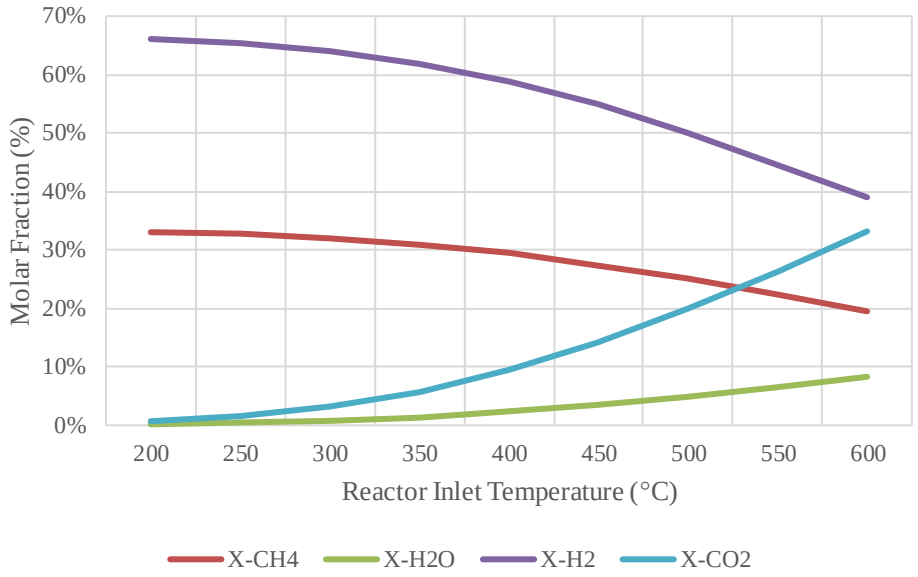

Figure 5.2 Effect of Sabatier reactor temperature on the molar fraction of species

Relationship between the water formed as a result of the Sabatier reaction and the reactor temperature at Figure 5.2. When the reactor temperature is assumed to be 200°C, the water yield at the end of the reaction is around 65%, but this decreases to around 39% as the temperature increases. As shown in Figure 5.2, increasing the temperature of the Sabatier reactor reduces the molar fraction of methane produced by the reaction compared to other types. Under initial conditions with a temperature of 200 °C, approximately 33% CH_4 is obtained. An increase in temperature resulted in a decrease in this ratio, which fell to 20% when the temperature reached 600 °C. The decrease in synthetic methane production, which is the main objective of the study, with increasing reaction temperature also reduces the thermal efficiency of the system.

5.4 Effect of Electrolyser Capacity on the System Efficiency

Another parametric analysis conducted within the scope of this study is the operating capacity of the PEM Electrolyser. Accordingly, the operating capacity of the Electrolyser was examined between 50% and 100%, and the net power produced by the system, the total energy and exergy efficiencies of the system were calculated.

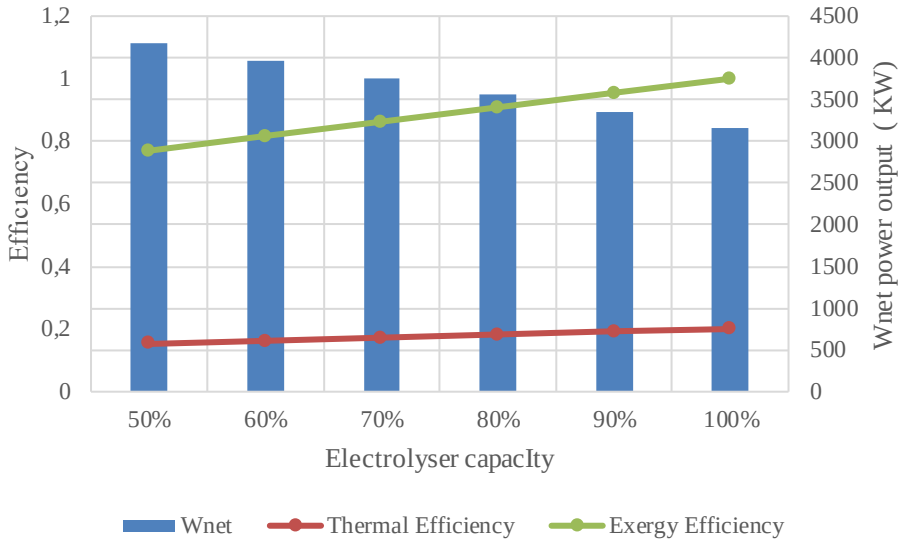

Figure 5.3 Effect of electrolyser capacity on the system efficiency

As shown in Figure 5.3, as the electrolysers operating capacity increases from 50% to 100%, the net power produced by the system decreases from 4167 kW to 3154 kW. This is because the energy required for the electrolyser to operate is supplied by the ORC system. However, the total thermal efficiency of the system also increases with the electrolyser capacity. This is explained by the fact that the increase in electrolyser capacity also increases methane gas production, which positively affects the thermal efficiency.

5.4 Effect of Production Well Temperature on the System Efficiency

The importance of reservoir temperature in geothermal energy systems has been explained in the previous sections. Reservoir temperature determines the engineering system of the geothermal plant to be established in that region. Within the scope of this study, the changes in net energy produced, total energy, and exergy efficiency with changes in reservoir temperature were also examined and are shown in Figure 5.4.

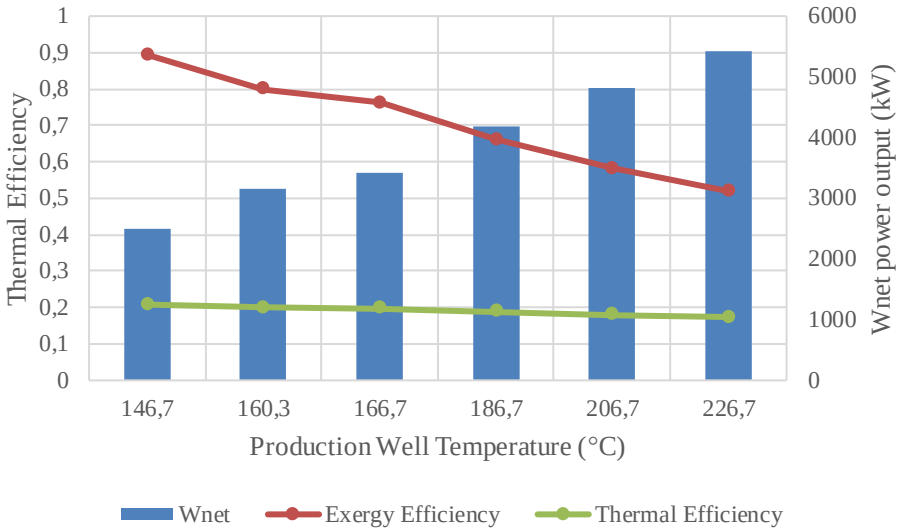

Figure 5.4 Effect of production well temperature on the net power output, exergy and thermal efficiency

As shown in Figure 5.4, an increase in reservoir temperature leads to a significant increase in net power output, but there is a general decrease in exergy and energy efficiency. The fundamental reason for this trend is that as the production well temperature increases from 146 to 226 °C , the energy input (heat input) increases much more rapidly, but the useful work obtained from the system increases at a slower rate relative to this increase as from 2.505 kW to 5.422kW. On the exergy side, irreversibility's (exergy losses) increase at high temperatures as from This causes useful work to increase at a lower rate relative to the large amount of energy entering the system, resulting in a decrease in exergy efficiency as from %80 to %51.

5.5 Exergy Destruction Calculation for Each Component at the System

Calculating exergy efficiency in a system indicates the quality of the energy produced within that system. Therefore, increasing exergy efficiency is highly beneficial for the system. Exergy destruction directly indicates the areas requiring improvement in the system by showing which component causes how much exergy loss. Within the scope of the study, the ACC, where heat loss is highest, is also the point of highest exergy destruction as %41 of the all system. In this process, which recovers the organic fluid by cooling it and returning it to the system, the heat released

is directly discharged into the atmosphere. By using a new heat exchanger, this lost heat can be recovered, thereby increasing system efficiency at this point.

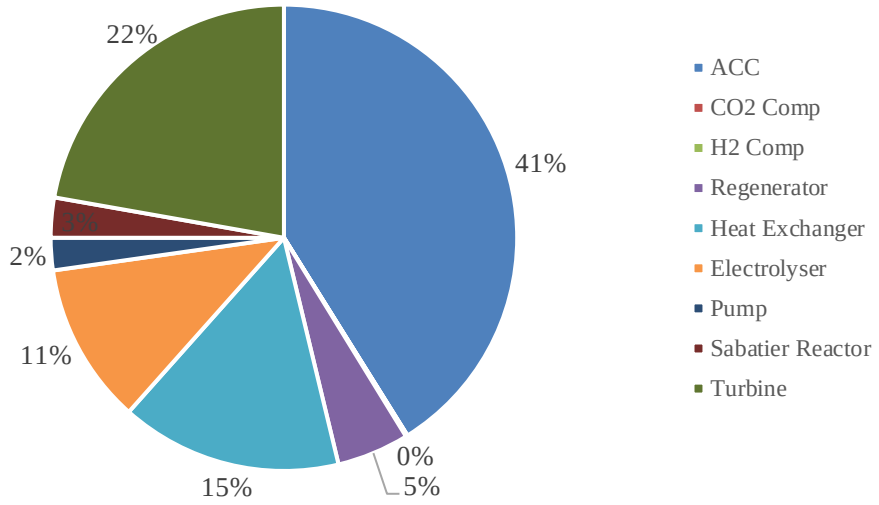

Figure 5.5 Exergy destructions ratios of each component in the integrated system

The exergy destruction rates of the components used in the system were presented as percentages in Figure 5. In Figure 5.6, the exergy destructions of all components are illustrated using a Sankey diagram.

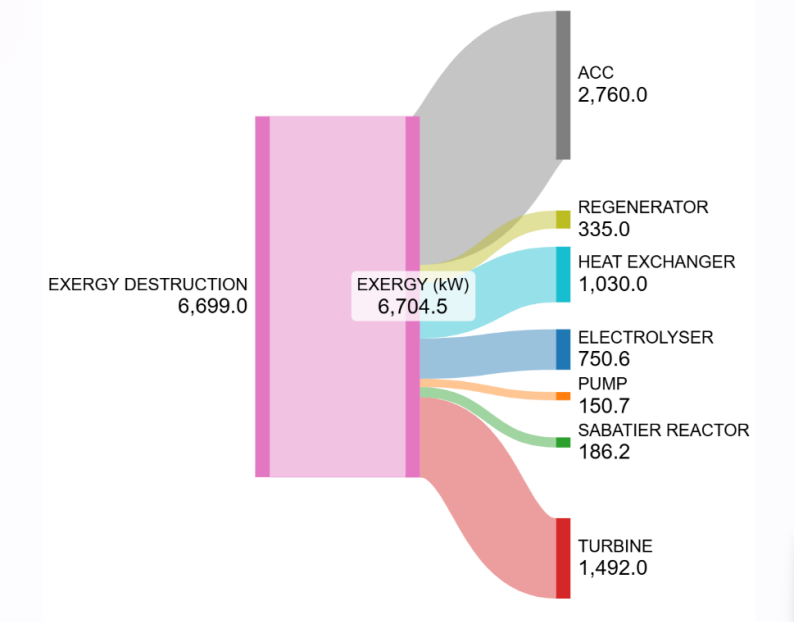

Figure 5.6 Exergy destruction rates of each component in integrated system on the Sankey Diagram

5.6 Techno-Economic Results of the System

In the previous section, equations taken from the literature regarding the costing of components used in the system created within the scope of this study were provided and shown in Table 4.1. Table 5.1 shows the calculated costs of these components.

Table 5.1 Components purchase cost calculations

Component	**Purchase Cost**
ORC Heat Exchanger	67,520$
Turbine+ Generator	385,000$
Regenerator	23,200$
ACC	640,000$
Pump	16,328$
CO_2 Compressor	1,000$
H_2 Compressor	4,500$
PEM	3,000,000$
Heat Exchanger Sabatier	25,000$
Sabatier Reactor	2,269,00$
CO_2 Capture System	60,000$
Contingencies	2,500,000$
Construction & Building Costs	8,000,000$

The cost of methane gas obtained from the system created is quite important for the efficiency of the study. At this point, it is necessary to perform the LCOM calculation shown in Equation 4.6 in the previous section and compare it with sources in the

literature. Accordingly, LCOM was found to be $2.6/kg within the scope of the study. The LCOM values in similar studies found in the literature are shown in Table 5.2. In the first two systems compared in this study, the electrolyzer is powered by electricity generated from solar and wind energy, while the required CO_2 is supplied through external procurement. In another system, the electrolyzer is instead powered by electricity drawn from the grid, with methanation again carried out using purchased CO_2.

Table 5.2 Comparison of LCOM values of this study with values found in the literature (Breiki., 2023)

LCOM (This study)	**Unit**	**LCOM (Literature)**	**Unit**
2.6	$/kg	4-4.9	$/kg
		0.56-3.4	$/kg
		1.16-2.07	$/kg
		1.66-2.45	$/kg

Another method used to measure the economic viability of the system is the calculation of the SPP. The method for calculating the SPP is shown in Equation 4.8 in Chapter 4. The SPP period of the system created within the scope of this study was calculated as 8.59 years. Thus, the total investment cost of the system is recovered in approximately 8.5 years, and the system continues to generate profit until the end of its life.

CHAPTER SIX
CONCLUSIONS

This thesis investigates a system integrated with a geothermal power plant that produces synthetic methane based on fundamental scientific principles. Subsequently, thermodynamic models were developed and thoroughly detailed for the ORC-type geothermal power plant supplying energy to the system, the PEM-type electrolyzer fulfilling the hydrogen demand, and the Sabatier reactor, where synthetic methane production occurs. All thermodynamic models developed within the scope of this study were solved using the EES program. The parametric effect of the organic fluid type used in the ORC on net power generation and total system efficiency was investigated. The thermal efficiency and net power output of the ORC system were calculated for different organic working fluids, including Isobutane, R124, R290, R134a, R227, and R152. Since the geothermal reservoir temperature varies depending on the region, the thermal efficiency, exergy, and net power generation were calculated for a temperature range of approximately 145–225 °C. Furthermore, the Sabatier reactor temperature was also studied parametrically, and the composition percentages of the resulting gases were compared across different reactor temperatures. Specifically, when the reactor temperature varied between 200 °C and 600 °C, the molar fraction of methane in the produced synthetic gas was calculated. The exergy destructions of all components used in the system were also evaluated under steady-state conditions, and the components requiring optimization were identified to enhance the overall system efficiency. Additionally, the integrated system was analyzed from a techno-economic perspective. Literature sources were reviewed to determine the costs of the system components, and the obtained costs were presented in detail. This section presents the necessary equations and methodologies used to calculate the Levelized Cost of Methane (LCOM) and the Simple Payback Period (SPP), which is expressed in years,

- The type of organic fluid used in ORC can significantly affect system efficiency and net power output. The highest efficiency is achieved with R290 gas, while the lowest efficiency is achieved with isobutane gas. When R290 gas is used, system efficiency is 20%, but when isobutane is used as

an organic fluid in the ORC system, total system efficiency drops to around 13%.

- In addition to the efficiency calculation in classic ORC systems, including the efficiency calculation of the gases coming out of the Sabatier reactor causes significant changes in the total system efficiency. Specifically, incorporating the methane gas obtained from the Sabatier reactor into the system efficiency calculation results in an efficiency increase of approximately 6%.
- The temperature value of the Sabatier reactor has a considerable effect on synthetic methane production efficiency. With an increase in temperature, the ratio of methane gas in the outgoing gases decreases; while the CH_4 ratio is at 33% levels at 200°C, efficiency drops below 20% when the temperature reaches 600°C.
- The electrolyser's operating capacity is assumed to be 100%. However, through parametric studies, this ratio has been varied between 50% and 100%. As the electrolyser capacity increases, the net power output decreases, but thermal efficiency increases. This is due to the increased amount of methane gas produced in the Sabatier reactor. When the electrolyzer capacity is assumed to be 100%, the system efficiency is at the 20% level, but when the electrolyzer capacity is reduced, the system efficiency drops to around 15%.
- Although exergy efficiency does not change significantly with an increase in electrolyser capacity, it shows a decrease. When the electrolyzer capacity is at 0%, the exergy efficiency is 39%. When this ratio reaches 100%, the exergy efficiency is calculated as 36%.
- An increase in reservoir temperature leads to an increase in net power produced. However, thermal efficiency and exergy efficiency show a decrease. The reason for this is that the amount of heat entering the system increases more than the net power produced, resulting in a decrease in system efficiency. The reservoir temperature was studied parametrically between 145 and 226°C. When the reservoir temperature was 145°C, the net power generated was 1252 kW. When the reservoir temperature rose to

226°C, this value reached 5422 kW. Thermal efficiency decreased from 22% to 17% and exergy efficiency decreased from 33% to 28% with the same reservoir temperature change.

- The exergy losses of the components used in the study were calculated, and the highest loss was observed in the ACC. The reason for this is that the air used to cool the organic fluid is released directly into the atmosphere. 41% of the total exergy destruction in the system occurred in the ACC.
- To calculate the economic sustainability and efficiency of the study, an LCOM calculation was performed, and LCOM was found as $2.6/kg. Values found in the literature are again indicated, and the value of $2.6/kg is sustainable. In the literature, this ratio reaches up to 4.9 $/kg in LCOM calculations.
- The return on investment for the system was calculated to be 8.59 years. Considering the system's lifespan to be 20 years, a system design that are detailed profitable for many years has been created.

This study is expected to contribute to both the academic community and the energy sector by demonstrating the techno-economic feasibility of synthetic methane production integrated with geothermal power plants. The findings provide valuable insights for policymakers and investors by highlighting the potential of coupling renewable energy with carbon utilization technologies to support decarbonization strategies. Furthermore, the research offers a methodological framework that can be applied to similar energy systems, enabling comparative evaluations and optimization studies. Future work may focus on experimental validation of model assumptions, integration with other renewable sources such as solar or wind, and the development of advanced control strategies to enhance overall system efficiency and economic competitiveness.

REFERENCES

Aksoy, N., Gok, O. S., Mutlu, H., & Kilinc, G. (2015, April). CO2 emission from geothermal power plants in Türkiye. In Proceedings World Geothermal Congress (p. 2015).

Al-Breiki, M., & Bicer, Y. (2023). Techno-economic evaluation of a power-to-methane plant: Levelized cost of methane, financial performance metrics, and sensitivity analysis. *Chemical Engineering Journal*, 471, 144725.

Aliyu, S., & Garba, M. M. (2019). Review on current global geothermal energy potentials and the future prospects. Int. J. Adv. Sci. Eng, 5(4), 10-31695.

Archer, D. (2011). Global warming: Understanding the forecast. John Wiley & Sons.

Atak, Y. N., Ince, A. C., Colpan, C. O., Iulianelli, A., Serincan, M. F., & Pasaogullari, U. (2025). Thermoeconomic analysis of an integrated membrane reactor and carbon dioxide capture system producing decarbonized hydrogen. *Energy Conversion and Management*, *326*, 119506.

Axelsson, G. (2024). The future of geothermal energy. In Living with climate change (pp. 397-422). Elsevier.

Babatunde, A. F., & Sunday, O. O. (2018, September). A review of working fluids for organic Rankine cycle (ORC) applications. In IOP conference series: materials science and engineering (Vol. 413, p. 012019). IOP Publishing.

Bagher, A. M., Vahid, M., Mohsen, M., & Parvin, D. (2015). Hydroelectric energy advantages and disadvantages. *American Journal of Energy Science*, 2(2), 17-20.

Bahrami, M., Hamidi, A. A., & Porkhial, S. (2013). Investigation of the effect of organic working fluids on thermodynamic performance of combined cycle Stirling-ORC. *International Journal of Energy and Environmental Engineering*, 4(1), 12.

Ball, M., & Wietschel, M. (Eds.). (2009). The hydrogen economy: opportunities and challenges.

Bertani, R. (2012). Geothermal power generation in the world 2005–2010 update report. Geothermics, 41, 1-29.

Bhandari, R., Trudewind, C. A., & Zapp, P. (2014). Life cycle assessment of hydrogen production via electrolysis–a review. *Journal of cleaner production*, 85, 151-163.

Bhuvanendran Nair Jayakumari, A., Malik, N. G., Mittal, G., Martelo, D., Kale, N., & Paul, S. (2023). A review on geothermal heat exchangers: Challenges, coating methods, and coating materials. Coatings, 13(12), 1988.

Bowen, R. (2012). Geothermal resources. Springer Science & Business Media.

Brinkmann, R. (Ed.). (2023). The Palgrave handbook of global sustainability. Springer Nature.

Cariaga, C., Cariaga, C., & Cariaga, C. (2025, January 20). ThinkGeoEnergy's Top 10 geothermal countries 2024 – Power. Think GeoEnergy - Geothermal Energy News.

Cattiaux, J., Ribes, A., & Cariou, E. (2024). How extreme were daily global temperatures in 2023 and early 2024. *Geophysical Research Letters*, 51(19), e2024GL110531.

Çelebi, C., Altınışık, H., Atak, Y. N., Colpan, C. O., & Devrim, Y. (2024). Hydrogen production: Electrolysis methods.

Chemical Engineering. (2025). Plant Cost Index (CEPCI) historical values. Retrieved September 28, 2025, https://www.chemengonline.com/Assets/File/CEPCI_1_01

Choi, C., Khuenpetch, A., Zhang, W., Yasuda, S., Lin, Y., Machida, H., ... & Norinaga, K. (2021). Determination of Kinetic Parameters for CO_2 Methanation (Sabatier Reaction) over Ni/ZrO_2 at a Stoichiometric Feed-Gas Composition under Elevated Pressure.

Chowdhury, A. S., & Ehsan, M. M. (2023). A critical overview of working fluids in organic rankine, supercritical rankine, and supercritical brayton cycles under various heat grade sources. *International Journal of Thermofluids*, 20, 100426.

Dagdas, A. (2007). Performance analysis and optimization of double-flash geothermal power plants.

Dhillon, B. S. (2009). Life cycle costing for engineers. Crc Press.

Dincer, I., & Rosen, M. A. (2012). Exergy: energy, environment and sustainable development. Newnes.

Dincer, I., & Zamfirescu, C. (2011). Sustainable energy systems and applications. Springer Science & Business Media.

Direct CO_2 hydrogenation to methane or methanol from post-combustion exhaust streams – A thermodynamic study. Journal of Natural Gas Science and Engineering

Du, N., Roy, C., Peach, R., Turnbull, M., Thiele, S., & Bock, C. (2022). Anion-exchange membrane water electrolyzers. *Chemical reviews*, *122*(13), 11830-11895.

Efeler Geothermal Power Plant Expansion - NS Energy. (2019, August 20). NS Energy. https://www.nsenergybusiness.com/projects/efeler-geothermal-power-plant/

EGEC - European Geothermal Energy Council. (2025, July 11). EGEC Geothermal Market Report 2024 - Key Findings now available! - EGEC - *European Geothermal Energy Council*. https://www.egec.org/media-publications/egec-market-report-2024-key-findings/

El Shinawi, A., Kuriqi, A., Zelenakova, M., Vranayova, Z., & Abd-Elaty, I. (2022). Land subsidence and environmental threats in coastal aquifers under sea level rise and over-pumping stress. Journal of Hydrology, 608, 127607.

Electrolyzers and renewable hydrogen production. RPOW. (2025, May 22). https://rpow.es/electrolyzers-key-to-the-production-of-renewable-hydrogen/

Ems power machines (2025, April 4). ORC Turbine - Organic Rankine Cycle - EMS Power machines. EMS Power Machines - Steam Turbines, ORC Turbines, Wood

Gasifiers, Diesel and Wood Powered Generators, Electric and Vibration Motors. https://ems-powermachines.com/orc-turbine/

Energy, U. (2004). Energy efficiency and renewable energy. US Government, Department of Energy, Tech. Rep., 2008, dOE/GO-102008, 2567.

Executive summary – The Future of Geothermal Energy – Analysis - IEA. (n.d.). IEA. https://www.iea.org/reports/the-future-of-geothermal-energy/executive-summary

Fetting, C. (2020). The European green deal. ESDN report, December, 2(9), 53.

Frey, M., van der Vaart, J., Bär, K., Bossennec, C., Calcagno, P., Dezayes, C., & Sass, I. (2023). Techno-economic assessment of geothermal resources in the variscan basement of the northern upper rhine Graben. *Natural Resources Research*, 32(1), 213-234.

Fridleifsson, I. B., Bertani, R., Huenges, E., Lund, J. W., Ragnarsson, A., & Rybach, L. (2008). The possible role and contribution of geothermal energy to the mitigation of climate change. In IPCC scoping meeting on renewable energy sources: Proceedings (pp. 59-80). Intergovernmental Panel on Climate Change.

Fridriksson, T., Mateos, A., Audinet, P., & Orucu, Y. (2016). Greenhouse gases from geothermal power production.

Garg, P., Kumar, P., Srinivasan, K., & Dutta, P. (2013). Evaluation of isopentane, R-245fa and their mixtures as working fluids for organic Rankine cycles. *Applied Thermal Engineering*, 51(1-2), 292-300.

Geothermal energy: Council calls for faster deployment. (2024, December 16). Consilium.https://www.consilium.europa.eu/en/press/pressreleases/2024/12/16/geothermal-energy-council-calls-for-faster-deployment/

Ghalandari, M., Irandoost Shahrestani, M., Maleki, A., Safdari Shadloo, M., & El Haj Assad, M. (2021). Applications of intelligent methods in various types of heat exchangers: a review. *Journal of Thermal Analysis and Calorimetry*, 145(4), 1837-1848.

Götz, M., Lefebvre, J., Mörs, F., Koch, A. M., Graf, F., Bajohr, S., ... & Kolb, T. (2016). Renewable Power-to-Gas: *A technological and economic review. Renewable energy*, 85, 1371-1390.

Grigoriev, S. A., Fateev, V. N., Bessarabov, D. G., & Millet, P. (2020). Current status, research trends, and challenges in water electrolysis science and technology. *International Journal of Hydrogen Energy*, 45(49), 26036-26058.

Gutiérrez-Negrín, L. C. (2024). Evolution of worldwide geothermal power 2020–2023. Geothermal Energy, 12(1), 14.

Hassan, H. (2022). Fundamentals of geothermal energy extraction. In Utilization of Thermal Potential of Abandoned Wells (pp. 11-33). Academic Press.

Herath, H. M. D. P., Wijewardane, M. A., Ranasinghe, R. A. C. P., & Jayasekera, J. G. A. S. (2020). Working fluid selection of organic Rankine cycles. Energy Reports, 6, 680-686.

Hossain, S., Hossain, I., Jahangir, T., & Hasan, A. (2021). Direct utilization of geothermal energy with trends and potential role in a sustainable future outgrowth. ICRRD Qual Index Res J, 3, 11-24.

Huttrer, G. W. (1996). The status of world geothermal power production 1990–1994. Geothermics, 25(2), 165-187.

IEA (2023), Electricity Market Report 2023, IEA, Paris https://www.iea.org/reports/electricity-market-report-2023, Licence: CC BY 4.0

Ikechukwu, I. C. (2021). Geothermal Energy: A Review. *International Journal of Engineering Research & Technology*, 10(03).

IOGP Europe. (2025, August 26). Joint EGEC-IOGP Europe recommendations: Accelerating the deployment of Geothermal in Europe - IOGP Europe. https://iogpeurope.org/resource/joint-egec-iogp-europe-recommendations-accelerating-the-deployment-of-geothermal-in-europe/

Jalili, M., Holagh, S. G., Chitsaz, A., Song, J., & Markides, C. N. (2023). Electrolyzer cell-methanation/Sabatier reactors integration for power-to-gas energy storage: Thermo-economic analysis and multi-objective optimization. Applied Energy, 329, 120268.

Kabeyi, M. J. B. (2019). Geothermal electricity generation, challenges, opportunities and recommendations. *International Journal of Advances in Scientific Research and Engineering* (ijasre), 5(8), 53-95.

Karellas, S., & Braimakis, K. (2016). Energy–exergy analysis and economic investigation of a cogeneration and trigeneration ORC–VCC hybrid system utilizing biomass fuel and solar power. Energy conversion and management, 107, 103-113.

Katterbauer, K., Yılmaz, S., & Meral, G. (2025). A Comprehensive Analysis of Progress in the Renewable Energy Sector in Turkey. Journal of Recycling Economy & Sustainability Policy, 4(SI), 6-21.

Kaya, E., Zarrouk, S. J., & O'Sullivan, M. J. (2011). Reinjection in geothermal fields: A review of worldwide experience. *Renewable and sustainable energy reviews*, 15(1), 47-68.

Khan, M. A., Zhao, H., Zou, W., Chen, Z., Cao, W., Fang, J., ... & Zhang, J. (2018). Recent progresses in electrocatalysts for water electrolysis. *Electrochemical Energy Reviews*, 1(4), 483-530.

Kolditz, O., Jakobs, L. A., Huenges, E., & Kohl, T. (2013). Geothermal Energy: a glimpse at the state of the field and an introduction to the journal. Geothermal Energy, 1(1), 1.

Kristmannsdóttir, H., & Ármannsson, H. (2003). Environmental aspects of geothermal energy utilization. Geothermics, 32(4-6), 451-461.

Kuckshinrichs, W., Ketelaer, T., & Koj, J. C. (2017). Economic analysis of improved alkaline water electrolysis. Front Energy Res 2017; 5: 1.

Kumana, J. D. (1984). Cost update on specialty heat exchangers.

Kumar, S. S., & Himabindu, V. (2019). Hydrogen production by PEM water electrolysis–A review. *Materials Science for Energy Technologies* 2(3), 442-454.

Kumar, S. S., & Lim, H. (2022). An overview of water electrolysis technologies for green hydrogen production. Energy reports, 8, 13793-13813.

Laghari, A. S., Chandio, M. W., Kumar, L., & Haj Assad, M. E. (2024). Thermodynamic Performance Analysis of Geothermal Power Plant Based on Organic Rankine Cycle (ORC) Using Mixture of Pure Working Fluids. Energy Engineering, 121(8).

Lay, T., Hernlund, J., & Buffett, B. A. (2008). Core–mantle boundary heat flow. Nature geoscience, 1(1), 25-32.

Lee, K. C. (2001). Classification of geothermal resources by exergy. Geothermics, 30(4), 431-442.

Li, T., Gao, R., Gao, X., & Liu, Q. (2022). Synergetic Effect of Non-Condensable Gas and Steam Quality on the Production Capacity of Geothermal Wells and Geothermal Power Generation for Hot Dry Rock. Energies, 15(20), 7726.

Liang, Y., & Yu, Z. (2019). Working fluid selection for a combined system based on coupling of organic Rankine cycle and air source heat pump cycle. *Energy Procedia*, 158, 1485-1490.

Lund, J. W., Freeston, D. H., & Boyd, T. L. (2011). Direct utilization of geothermal energy 2010 worldwide review. Geothermics, 40(3), 159-180.

Mathiesen, B. V., Duić, N., Stadler, I., Rizzo, G., & Guzović, Z. (2012). The interaction between intermittent renewable energy and the electricity, heating and transport sectors. Energy, 48(1), 2-4.

Menéndez, J., Ordóñez, A., Álvarez, R., & Loredo, J. (2019). Energy from closed mines: Underground energy storage and geothermal applications. *Renewable and Sustainable Energy Reviews*, 108, 498-512.

Merbecks, T., Alfani, D., Bombarda, P., & Silva, P. (2024). On the thermodynamic and economic performance of binary power plant configurations for the exploitation of two-phase geothermal resources. In PROCEEDINGS, 49th Workshop on Geothermal Reservoir Engineering Stanford University, Stanford, California, February 12-14, 2024 (pp. 1-12).

Molavi, J., & McDaniel, J. (2016). A review of the benefits of geothermal heat pump systems in retail buildings. Procedia Eng, 145, 1135-1143.

Molino, A., & Braccio, G. (2015). Synthetic natural gas SNG production from biomass gasification–Thermodynamics and processing aspects. Fuel, 139, 425-429.

Morgenthaler, S., Ball, C., Koj, J. C., Kuckshinrichs, W., & Witthaut, D. (2020). Site-dependent levelized cost assessment for fully renewable Power-to-Methane systems. Energy conversion and management, 223, 113150.

Nkinyam, C. M., Ujah, C. O., Asadu, C. O., & Kallon, D. V. (2025). Exploring geothermal energy as a sustainable source of energy: A systemic review. Unconventional Resources, 100149.

Omenikolo, A. I., Obasi, I. B., & Nleonu, E. C. (2020). Application of geothermal energy in agriculture: a review. Int J Eng Appl Sci Technol, 5(1), 666-673.

Owusu, P. A., & Asumadu-Sarkodie, S. (2016). A review of renewable energy sources, sustainability issues and climate change mitigation. Cogent Engineering, 3(1), 1167990.

Park, S., Langat, A., Lee, K., & Yoon, Y. (2021). Measuring the impact of risk on LCOE (levelized cost of energy) in geothermal technology. Geothermal Energy, 9(1), 27.

Parri, R., & Lazzeri, F. (2016). Larderello: 100 years of geothermal power plant evolution in Italy ın Geothermal Power Generation (pp. 537-590). Woodhead Publishing.

Rosen, M. A., & Dincer, I. (2001). Exergy as the confluence of energy, environment and sustainable development. Exergy, an international journal, 1(1), 3-13.

RPow - Empresa de Ingeniería en Sevilla. (2025, May 22). Electrolyzers and renewable hydrogen production. RPOW - Renewable Power Onwards.

Shiva Kumar, S., Ramakrishna, S. U. B., Srinivasulu Reddy, D., Bhagawan, D., & Himabindu, V. J. I. J. C. E. P. T. (2017). Synthesis of polysulfone and zirconium oxide coated asbestos composite separators for alkaline water electrolysis. Int. J. Chem. Eng. Process Technol, 3, 1035.

Sufyana, C. M., Akbar, F. T., & Srigutomo, W. (2023). Thermal modeling and simulation of a single-flash geothermal power plant involving non-condensable gas: a case study of Kamojang geothermal field in Garut, West Java, Indonesia. Geothermal Energy, 11(1), 6.

Svalova, V. (2018). Geothermal Energy. In Encyclopedia of Engineering Geology (pp. 411-417). Springer, Cham.

Swapnesh, A., Srivastava, V. C., & Mall, I. D. (2014). Comparative study on thermodynamic analysis of CO2 utilization reactions. *Chemical Engineering & Technology*, 37(10), 1765-1777.

Takano, H., Kirihata, Y., Izumiya, K., Kumagai, N., Habazaki, H., & Hashimoto, K. (2016). Highly active Ni/Y-doped ZrO2 catalysts for CO2 methanation. Applied Surface Science, 388, 653-663.

the system’s performance

Timmerhaus, K. D., & West, R. E. (2004). Plant design and economics for chemical engineers. McGraw-Hill.

Vafeas, N. A. (2021). Geothermal Energy: Barriers and Advantages to Adoption i n Ireland.

Vogt, C., Monai, M., Kramer, G. J., & Weckhuysen, B. M. (2019). The renaissance of the Sabatier reaction and its applications on Earth and in space. Nature catalysis, 2(3), 188-197.

Wang, B., Klemeš, J. J., Li, N., Zeng, M., Varbanov, P. S., & Liang, Y. (2021). Heat exchanger network retrofit with heat exchanger and material type selection: A review and a novel method. *Renewable and Sustainable Energy Reviews*, 138, 110479.

Wang, L., Dai, Z., Yao, L., Yang, L., & Jiang, W. (2024). The mitigation of carbon deposition for Ni-based catalyst in CO2 reforming of methane: A combined experimental and DFT study. Carbon Capture Science & Technology, 13, 100286.

Wisniak, J. (2005). Catalytic hydrogenation. Indian journal of chemical technology, 12(2), 232-243.

Xing, R., Jiang, Y., Li, J., Liu, P., Liu, Y., & Zhang, C. (2025). Ni/MgO-Al2O3 Catalysts for CO2 Methanation: Deactivation Mechanism Study. Industrial & Engineering Chemistry Research.

Yang, M. H., Liu, M. C., & Yeh, R. H. (2024). Investigation of low-GWP working fluids as substitutes for R245fa in organic Rankine cycle application. Heliyon, 10(14).

Yilmaz, C. (2020). Life cycle cost assessment of a geothermal power assisted hydrogen energy system. Geothermics, 83, 101737.

Zhang, F., Zhao, P., Niu, M., & Maddy, J. (2016). The survey of key technologies in hydrogen energy storage. International journal of hydrogen energy, 41(33), 14535-14552

Zycher, B. (2024). Response to the Office of Energy Efficiency and Renewable Energy.